Chapter 4: Deformation behavior and Tribo-Mechanical Properties of the Complex Eutectic Al-11Si-2.5Cu-0.6Fe alloy during Forging

4.1 Introduction

As discussed in the previous chapter that the presence of the coarse second particles in the Al matrix makes it unsuitable for bulk processing under various metal working conditions. The hard second particles initiate cracks in the samples during processing which further propagate with the deformation to form severe surface cracks in the test samples. Therefore, careful selection of the processing parameters such as processing temperature, lubrication, and deformation speed is required to obtain the desired results. In the present study, the amount of Si is reduced from 18 to 11wt.% in the Al-Si alloy to analyze the influence of Si on deformation behavior and tribo-mechanical properties of the alloy during bulk processing. The alloy complex eutectic Al-11Si-2.5Cu-0.6Fe (wt.%) alloy thus formed through open die, impression die and converging die sets under different processing conditions such as working temperature, aspect ratios/reduction ratios, and interfacial frictional conditions. It is expected that the present work provides valuable insight into understanding the deformation behavior and tribo-mechanical characteristics of the complex eutectic Al-11Si-2.5Cu-0.6Fe (wt.%) alloy under different processing conditions.

4.2 Results and Discussion

4.2.1 Microstructural features of the as-cast alloy

The x-ray diffraction (XRD) spectrum of the as-cast Al-11Si-2.5Cu-0.6Fe alloy is shown in Figure 4.1. The phases present in the alloys have been identified using the International Centre for Diffraction Data (ICDD) PDF database. The results reveal high-intensity peaks

of aluminum and silicon phases present in the XRD patterns. However, few low intensity of diffraction peaks also observed in the XRD pattern, and identified as β-$Al_{4.5}FeSi$ and Al_2Cu intermetallic compounds. These intermetallic compounds were formed due to the reaction between the alloying elements due to exposure of the higher temperature during casting. Since the alloy comprises of silicon, copper, and iron element, which formed different complex intermetallic phases of silicon, copper or iron during the process run over.

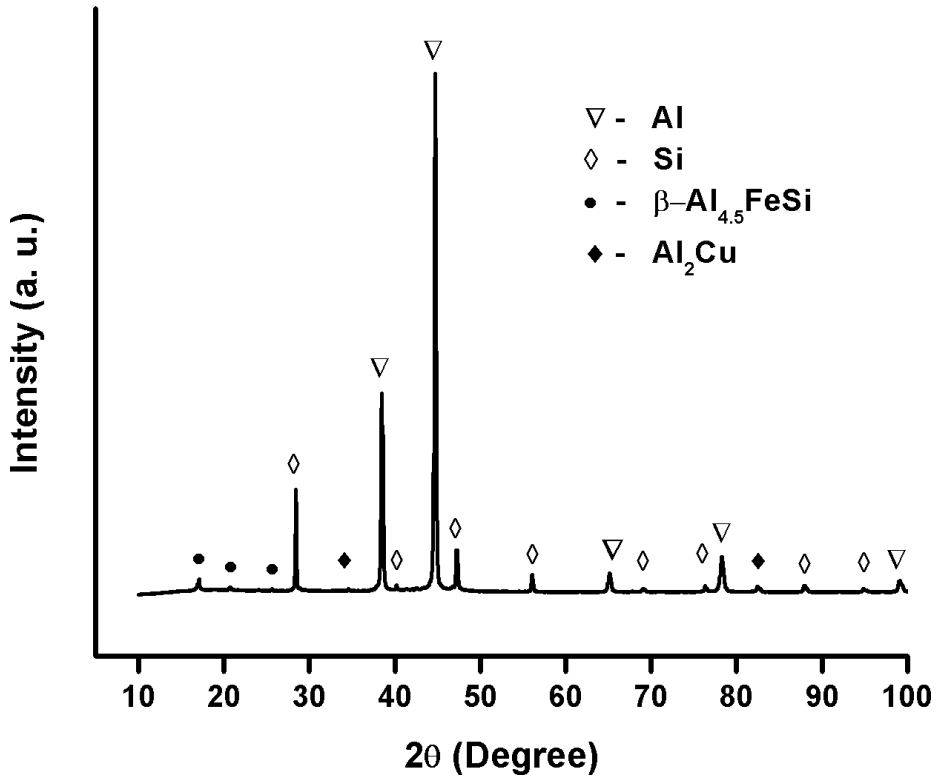

Figure 4.1 X-ray diffraction (XRD) patterns of the as-cast alloy

The EDAX spectrum of the as-cast alloy was taken from the area observed in the SEM images as shown in Figure 4.2. Figure 4.2(a) shows the EDAX spectrum of Si crystal. EDAX spectrum from Figures 4.2(b) and 4.2(c) also confirmed the formation of complex intermetallic phases (Al_2Cu and β-$Al_{4.5}FeSi$) which were plate type and coarse needle-shaped structured.

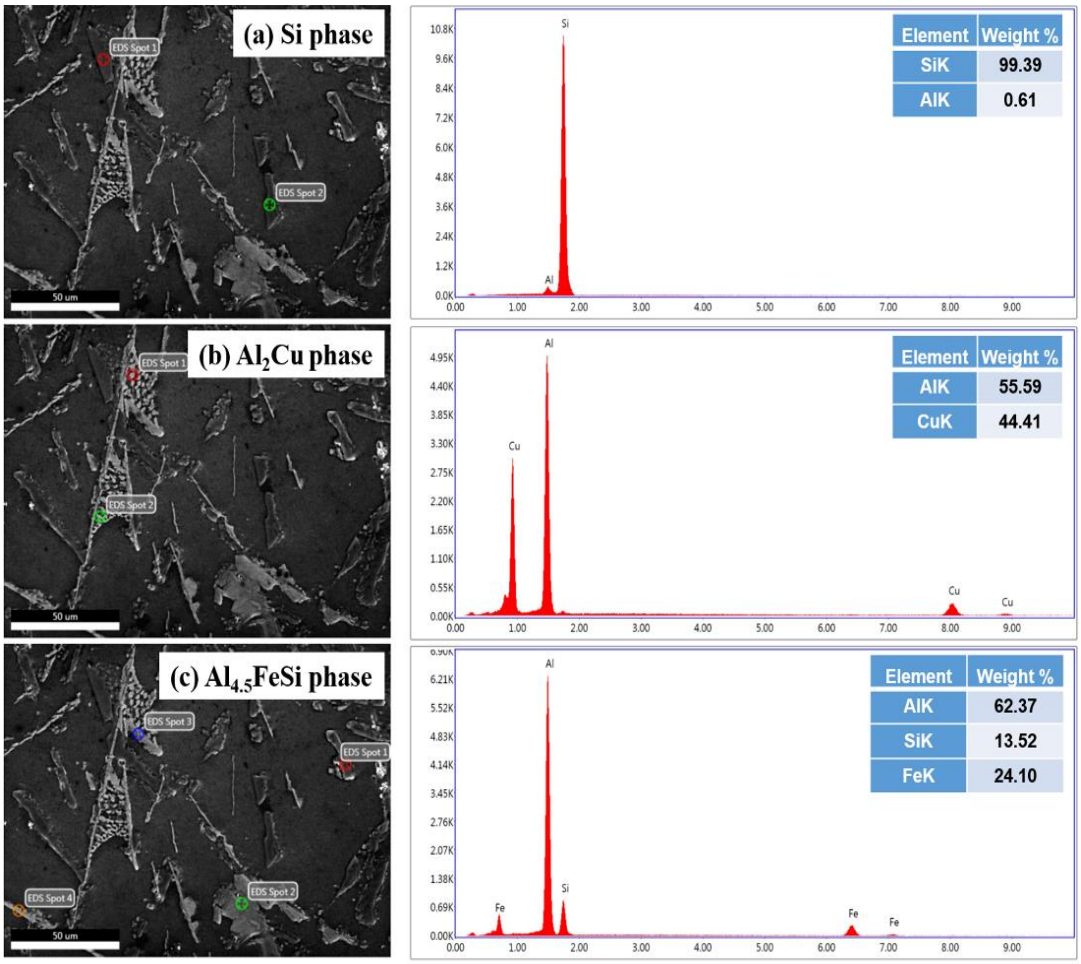

Figure 4.2 EDAX analysis of the as-cast alloy

Figure 4.3 shows the optical microstructure of the as-cast Al-11Si-2.5Cu-0.6Fe alloy. The microstructure reveals the presence of coarse and needle-shaped eutectic silicon along with few primary silicon particles randomly oriented in α-Al matrix. Mostly, the alloy with eutectic composition consists of α-Al and eutectic silicon particles while the presence of primary silicon particles indicate fast cooling rate during the solidification process. The skewed couple zone formed during solidification reflects the presence of primary Si particles in the eutectic Al-Si alloy (Jigajinni et al., 2013). The dark and bright color grains indicate the Si particles and intermetallic compounds respectively. These particles are irregular in shape and non-uniformly distributed in the α-Al matrix. The formation of such microstructural features due to non-uniform solidification during casting, result in coarse particulates of Si and intermetallics. The mean diameter and

standard deviation of the eutectic silicon particles were measured as 23.55 µm and 11.30 µm respectively, whereas 49.30 µm and 21.43 µm for primary Si particles. Such microstructural features deteriorate the mechanical and tribological properties of these alloy. Therefore, alteration is needed from coarse microstructural features to refined structure with uniform dispersion to achieve the desired engineering properties. Earlier, the several investigators have also shown a similar morphology in eutectic Al-Si alloy against different chemical compositions. It is revealed that the coarse α-Al dendrites along with needle-shaped eutectic Si particles in the cast alloy lower the engineering properties of the alloy (Kaya and Aker, 2017; Yang et al., 2018).

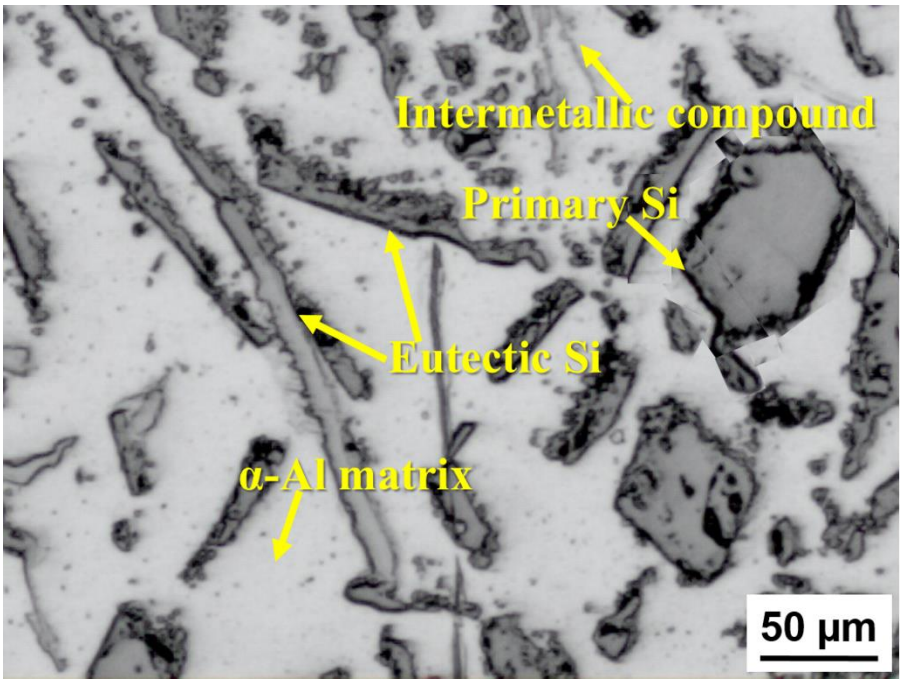

Figure 4.3 Optical microstructure of the as-cast alloy

4.2.2 Deformation behavior of the complex eutectic Al-11Si-2.5Cu-0.6Fe alloy forged under different die sets

Deformation behavior of the complex eutectic Al-11Si-2.5Cu-0.6Fe alloy was also investigated through the open, impression and converging dies forging.

4.2.2.1 Deformation behavior of the complex eutectic Al-Si alloy during open die forging

Figure 4.4 shows the three regimes of silicon-intermetallic particles distribution in the aluminum matrix during open die forging of Al-Si alloy. The results reveal that open die forging of the complex Al-11Si-2.5Cu-0.6Fe alloy test samples (h/d=1) developed surface cracks on the outer periphery in both room and elevated working temperatures (300°C), as shown in Figures 4.5(a-b). The severity of surface cracks was greater in test samples forged at room temperature than that of 300°C.

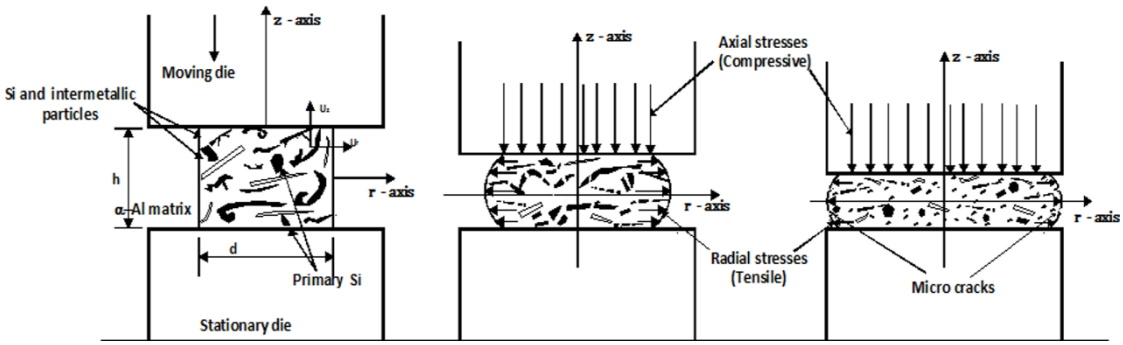

Figure 4.4 Three regimes of silicon-intermetallic particles distribution with aluminum matrix during open die forging of the complex Al-Si alloy

The complex alloy contains hard second phase particles comprising of the needle and plate shaped eutectic Si and complex intermetallic compounds along with coarse primary Si particles. Such microstructural features reduce the ductility and in turn the deformability of the alloy during bulk processing. During forging at room temperature the stress concentration developed between needle-shaped second phase particles and α-Al matrix results cracking which further propagates with deformation. Therefore, the alloy fails to sustain high axial (compressive), and radial (tensile) stresses during deformation and generates macro separation in interface region, which leads to severe surface cracks as shown in Figure 4.5(a).

The open die forging of the complex Al-Si alloy at 300°C generates the minute surface cracks in the preforms. Due to the incomplete recovery process between soft α-Al matrix

and second phase particles causes micro separation between liquid and solid regions. Therefore, it produces surface cracks on the outer periphery of the forged product as shown in Figure 4.5(b).

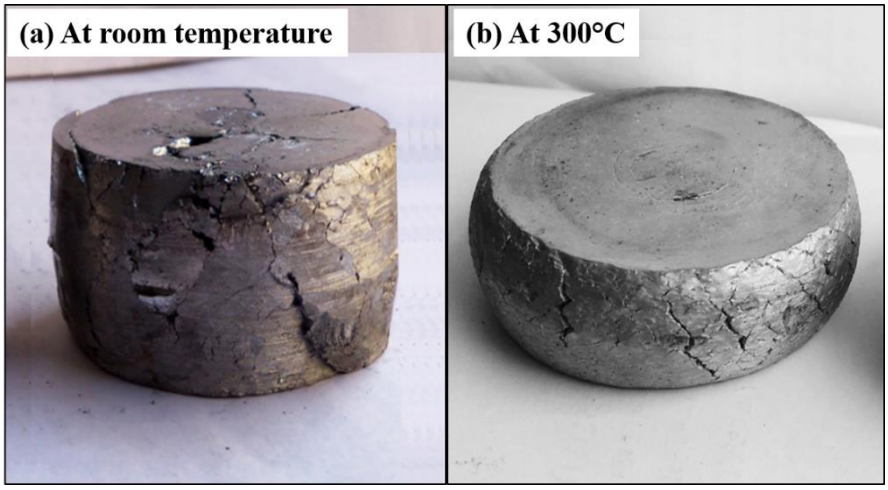

Figure 4.5 Open die forged products under different working condition (a) room temperature, and (b) 300°C

In view of the above discussion, it is established that the open die forging of the complex Al-11Si-2.5Cu-0.6Fe alloy is not feasible in both room and elevated temperatures.

4.2.2.2 Deformation behavior of the complex eutectic Al-Si alloy during impression die forging at room temperature

Figures 4.6(a-b) and 4.7 show the photograph of forged products and their corresponding forging load against aspect ratio under lubricated and unlubricated interfacial frictional conditions. The preform with an aspect ratio 1.00 shows minute cracks on equatorial surface after compression whereas preform with high aspect ratio (1.20) show severe surface cracks. The results also reveal that preform forged at unlubricated condition produces severe surface cracks as compared with lubricated condition. It may be due to lubrication which reduces friction between preform and die wall, and allow the metal flow during deformation. However, the preform with aspect ratio 0.80 undergoes controlled amount of axial (compressive) stresses, radial (tensile) stresses and also back

(compressive) stresses from die walls and consequently produce a forged product with very few minute surface cracks.

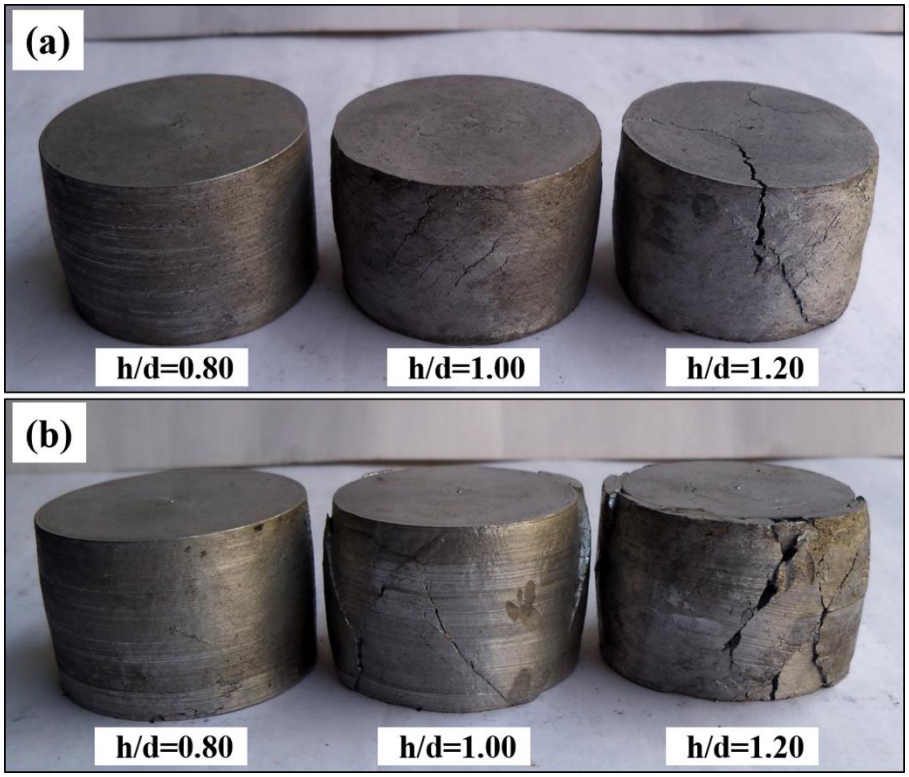

Figure 4.6 Photograph cold forged preform under interfacial frictional conditions with different aspect ratios (a) lubricated, and (b) unlubricated

Bulk processing of the complex eutectic Al-11Si-2.5Cu-0.6Fe alloy through impression die also produces surface cracks on the outer periphery of the forged products. In earlier, it was discussed that the radial stresses initiate stress concentration between second phase particles and α-Al matrix during the forging of the alloy at room temperature. As the deformation progressed, the preform got fractured and fragmented during processing and gradually fills the die impression. As evident in Figure 4.7, the unlubricated forging shows higher deformation load than the lubricated one. It may be due to the less surface movement between the die wall and preform. Results also reveal that the deformation load increases with an increase in aspect ratio in both frictional conditions. However, the preform with 1.20 aspect ratio show lower forging load, it may due to large fracture and fragmentation of the preform before die filling.

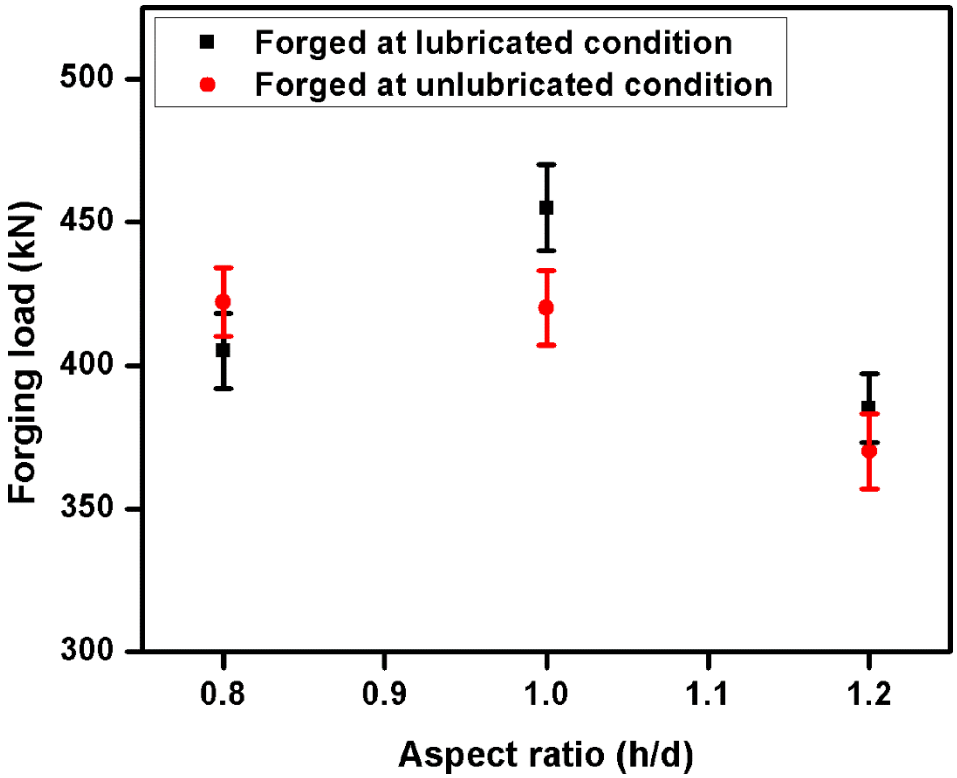

Figure 4.7 Variation of forging load with aspect ratio (h/d) at lubricated and lubricated conditions

In view of the above discussion, it is established that the impression die forging of the complex eutectic Al-11Si-2.5Cu-0.6Fe alloy is not feasible at room temperature and the preform got cracked during processing.

4.2.2.3 Deformation behavior of the complex eutectic Al-Si alloy during impression die forging at elevated working temperatures

Figures 4.8-4.9 and 4.10-4.11 show the photograph of forged products and their corresponding forging load under various processing conditions. Since coarse second phase particles enhance the hardness of the alloy and reduce the formability of the material during bulk processing. Therefore, the test samples got fractured during processing at the cold condition and consequently, the forging was tried at elevated temperature. Forging of the alloy at elevated temperature induced ductility during processing and thereby softening the alloy. Thus, defect free smooth products were obtained through forging of the alloy at elevated temperatures.

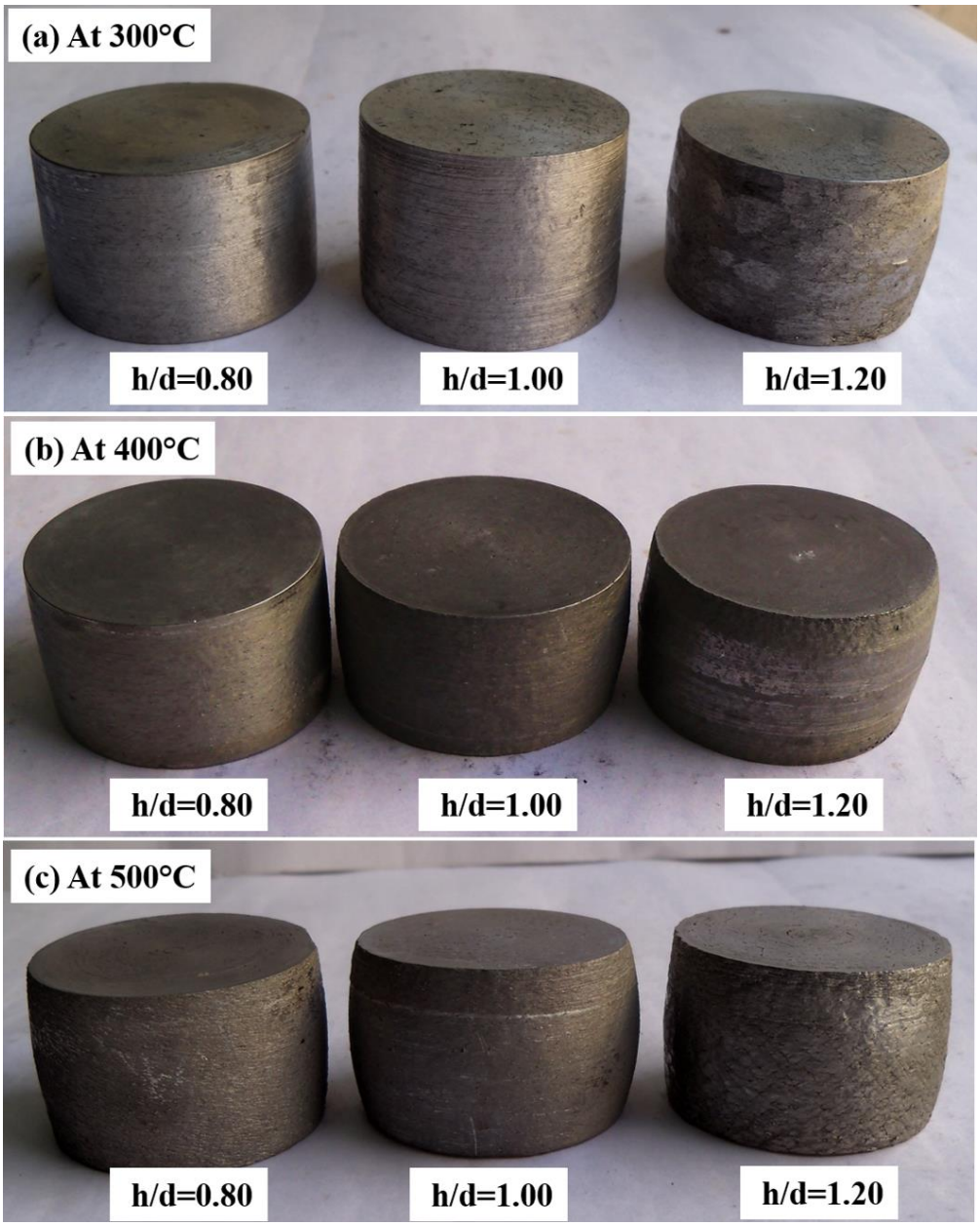

Figure 4.8 Photograph of impression die forged products under lubricated condition at elevated processing temperature (a) 300°C, (b) 400°C, and (c) 500°C

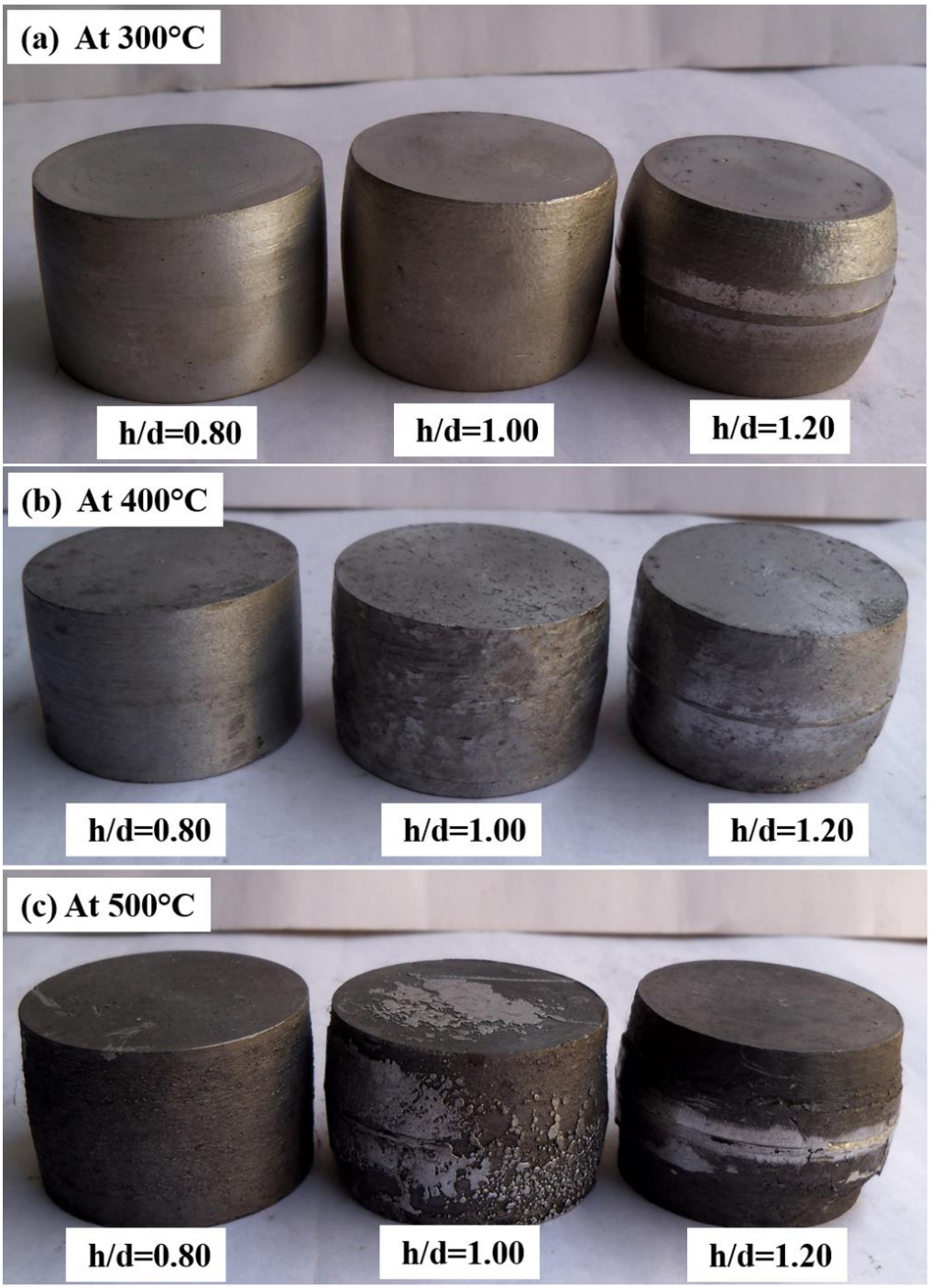

Figure 4.9 Photograph of impression die forged products under unlubricated condition at elevated processing temperature (a) 300°C, (b) 400°C, and (c) 500°C

Figures 4.10 and 4.11 show that less forging load was required to deform the Al-11Si-2.5Cu-0.6Fe alloy as compared to Al-18Si-2.5Cu-0.6Fe alloy due to low hardness value. The results also reveal that the forging load increases with the increase in the aspect ratios, while it reduces when working temperatures increases under both lubricated and unlubricated conditions. It may be due to percentage reduction increases and higher for

aspect ratio (35%), while degree of the softness increased as increases the working temperatures.

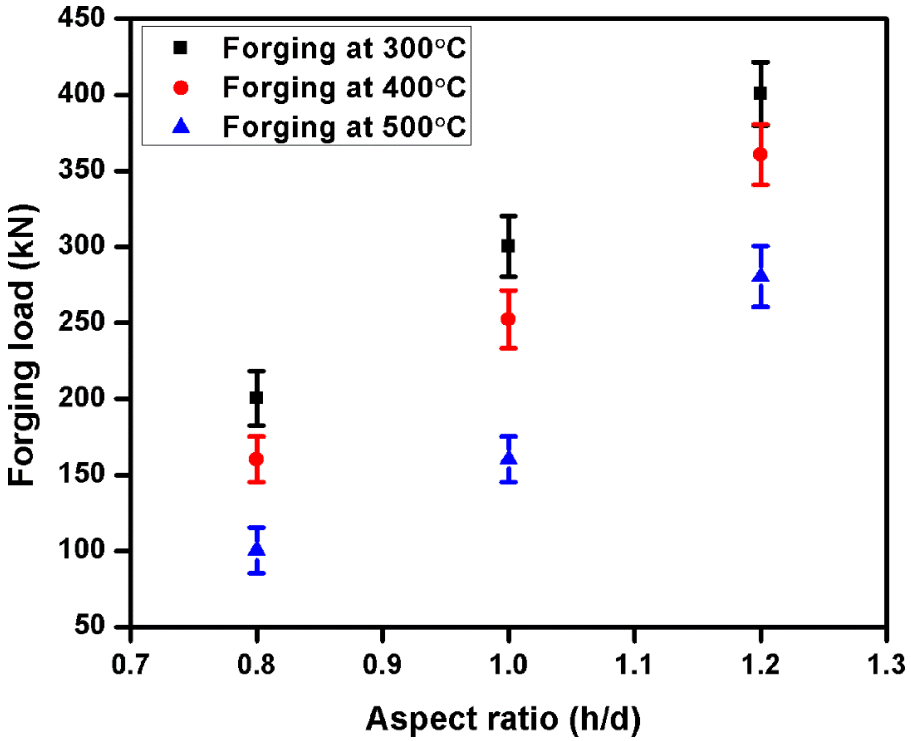

Figure 4.10 Variation of forging load with aspect ratio (h/d) at different working temperatures under lubricated condition

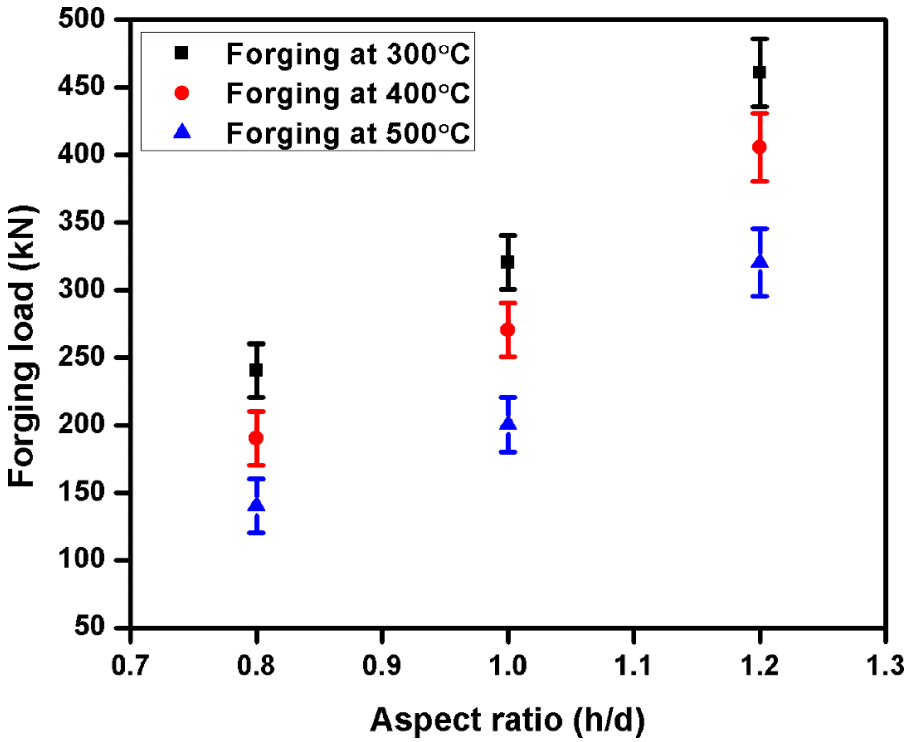

Figure 4.11 Variation of forging load with aspect ratio (h/d) at different working temperatures under unlubricated condition

In view of the above results, it is evident that the bulk processing of the complex eutectic Al-11Si-2.5Cu-0.6Fe alloy through impression die forging is feasible and defect free forged components can be produced.

4.2.2.4 Deformation behavior of the complex eutectic Al-Si alloy during converging die forging

The converging die forging of the complex eutectic Al-11Si-2.5Cu-0.6Fe was performed under similar processing conditions as mentioned in section 3.2.2.4. Here, the billets forged with reduction ratios of 1.5 and 2.0 at 300, 400 and 500°C working temperatures. Figures 4.12(a-c) and 4.13 show the photograph of forged products and their corresponding forging load under various processing conditions. The bulk processing of Al-11Si-2.5Cu-0.6Fe alloy through converging die also produced defect free forged products. The billets forged at 300°C and low reduction ratio (1.5) show better surface finish as compared with other processing conditions as shown in Figure 4.10.

Figure 4.12 Photographs of forged products at various elevated working temperatures (a) 300°C, (b) 400°C, and (c) 500°C

Figure 4.13 reveals that forging load decreased when increase the working temperatures, while it increased when increase the reduction ratio. Due to heavy deformation and consequent flow of the material through converging section the soft α-Al matrix

deformed plastically whereas hard second phase particles got fragmented, and uniformly dispersed in the matrix.

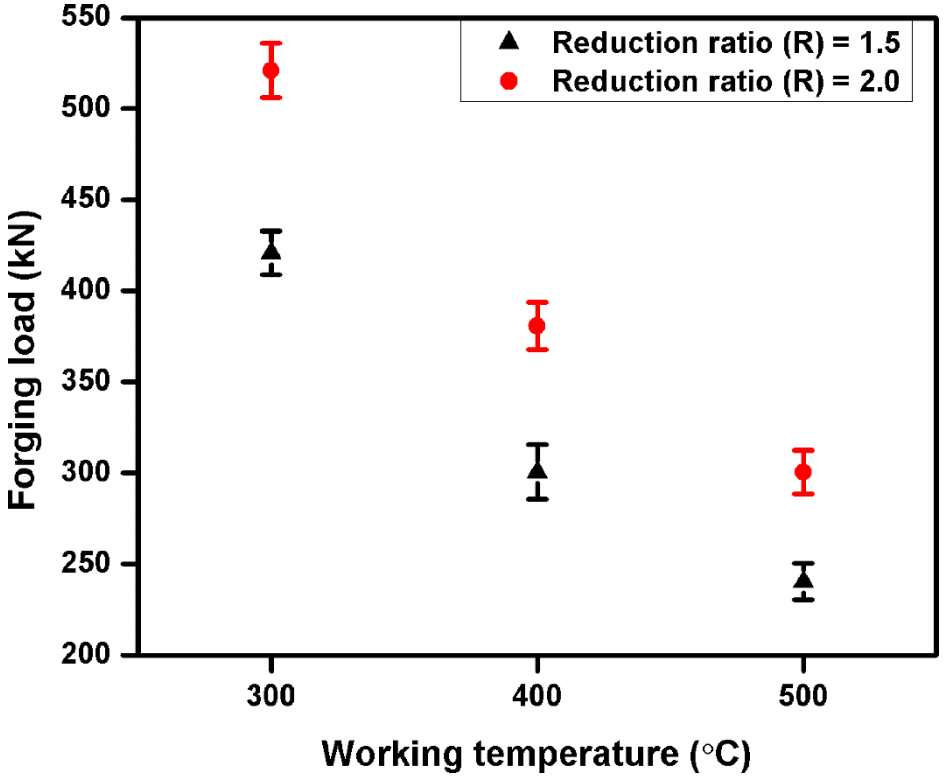

Figure 4.13 Forging load plotted against working temperatures for different reduction ratios

4.2.3 Microstructural features of the forged complex eutectic Al-11Si-2.5Cu-0.6Fe alloy

Microstructural studies of the forged products were performed as per the procedures mentioned earlier in the section 2.6. Figures 4.14-4.16 and 4.17 depict the optical micrograph and Tables 4.1 and 4.2 show the variation in average grain size of the Si particles in forged samples with the different aspect ratio (h/d) and working temperatures under lubricated and unlubricated conditions, respectively. The Figures 4.17(a-f) show optical micrographs and Table 4.3 shows the variation in average grain size of the Si particles in forged samples with different reduction ratios and working temperatures.

Table 4.1 Variation of average grain size of the eutectic silicon particle in forged samples under different processing conditions

Aspect Ratio (h/d)	Mean diameter/Standard deviation of the eutectic Si particles under different forging temperatures (μm)					
	300°C		400°C		500°C	
	Lub. cond.	Unlub. cond.	Lub. cond.	Unlub. cond.	Lub. cond.	Unlub. Cond.
1.20	9.35/3.40	9.95/3.20	8.55/3.04	9.15/3.07	8.86/3.31	10.47/3.75
1.00	9.91/3.64	11.35/4.35	8.88/3.56	10.5/3.70	9.29/3.65	10.30/4.06
0.80	12.30/4.53	12.90/4.60	10.62/3.85	11.65/4.15	9.08/3.73	10.45/4.72

Table 4.2 Variation of average grain size of the primary silicon particle in forged samples under different processing conditions

Aspect Ratio (h/d)	Mean diameter/Standard deviation of primary Si particle under different forging temperatures (μm)					
	300°C		400°C		500°C	
	Lub. cond.	Unlub. cond.	Lub. cond.	Unlub. cond.	Lub. cond.	Unlub. Cond.
1.20	15.77/5.50	19.51/5.90	13.30/3.67	15.47/5.42	30.28/11.08	34.54/10.60
1.00	21.05/9.17	25.77/10.37	16.80/5.25	16.97/5.80	34.30/12.50	35.56/12.62
0.80	26.85/12.13	29.76/7.38	17.23/5.56	18.54/6.63	42.08/13.09	45.08/13.65

Table 4.3 Variation in average grain size Si particles in forged samples at different processing temperatures

Forging temperature (°C)	Eutectic Si particles size at different reduction ratio (R)				Primary Si particles size at different reduction ratio (R)			
	R=1.5		R=2		R=1.5		R=2	
	Mean dia. (μm)	Stand. dev. (μm)	Mean dia. (μm)	Stand. dev. (μm)	Mean dia. (μm)	Stand. dev. (μm)	Mean dia. (μm)	Stand. dev. (μm)
300	9.62	3.84	9.10	3.10	15.35	3.93	15.05	4.15
400	9.10	3.20	8.20	2.90	13.95	3.35	13.20	3.19
500	10.21	3.65	9.64	3.20	28.65	10.15	25.48	9.46

The results show the microstructural refinement in forged samples during processing of the alloy through impression die as well as converging die at 300, 400, and 500°C temperatures. The extent of microstructural refinement was more in converging die forging due to severe deformation of the alloy during processing.

The microstructural refinement mechanism in forged alloy contains precipitation of elemental silicon and intermetallic compounds containing Cu, and Fe giving rise to finer precipitates of Si and the intermetallic compounds during homogenization before forging. While coarse eutectic and primary Si along with complex intermetallic phases got fractured and fragmented and uniformly dispersed in the α-Al matrix due to applied deformation load as shown in Figures 4.14-4.17.

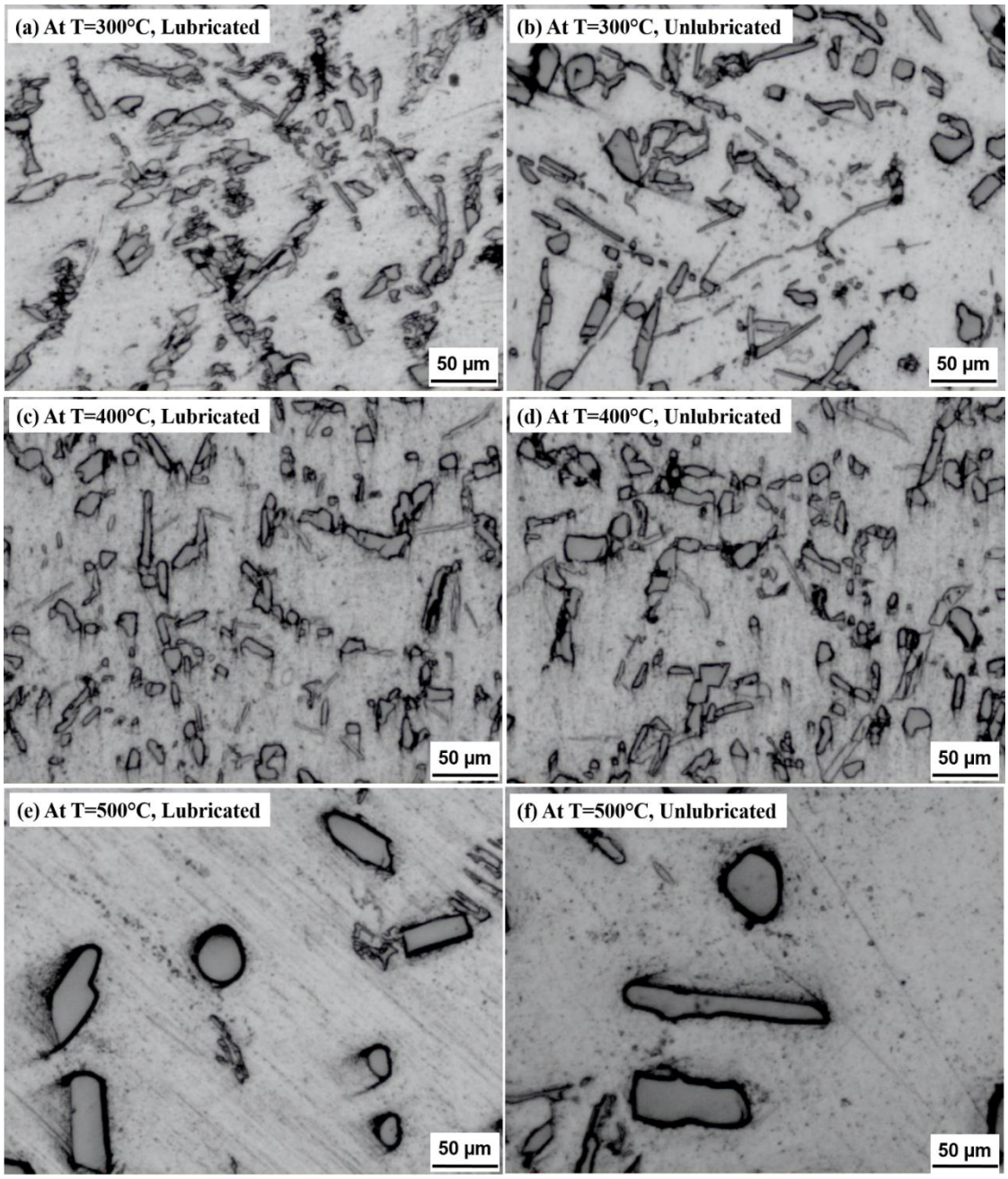

Figure 4.14 Optical microstructure of the forged samples at aspect ratio 1.20 under lubricated and unlubricated conditions

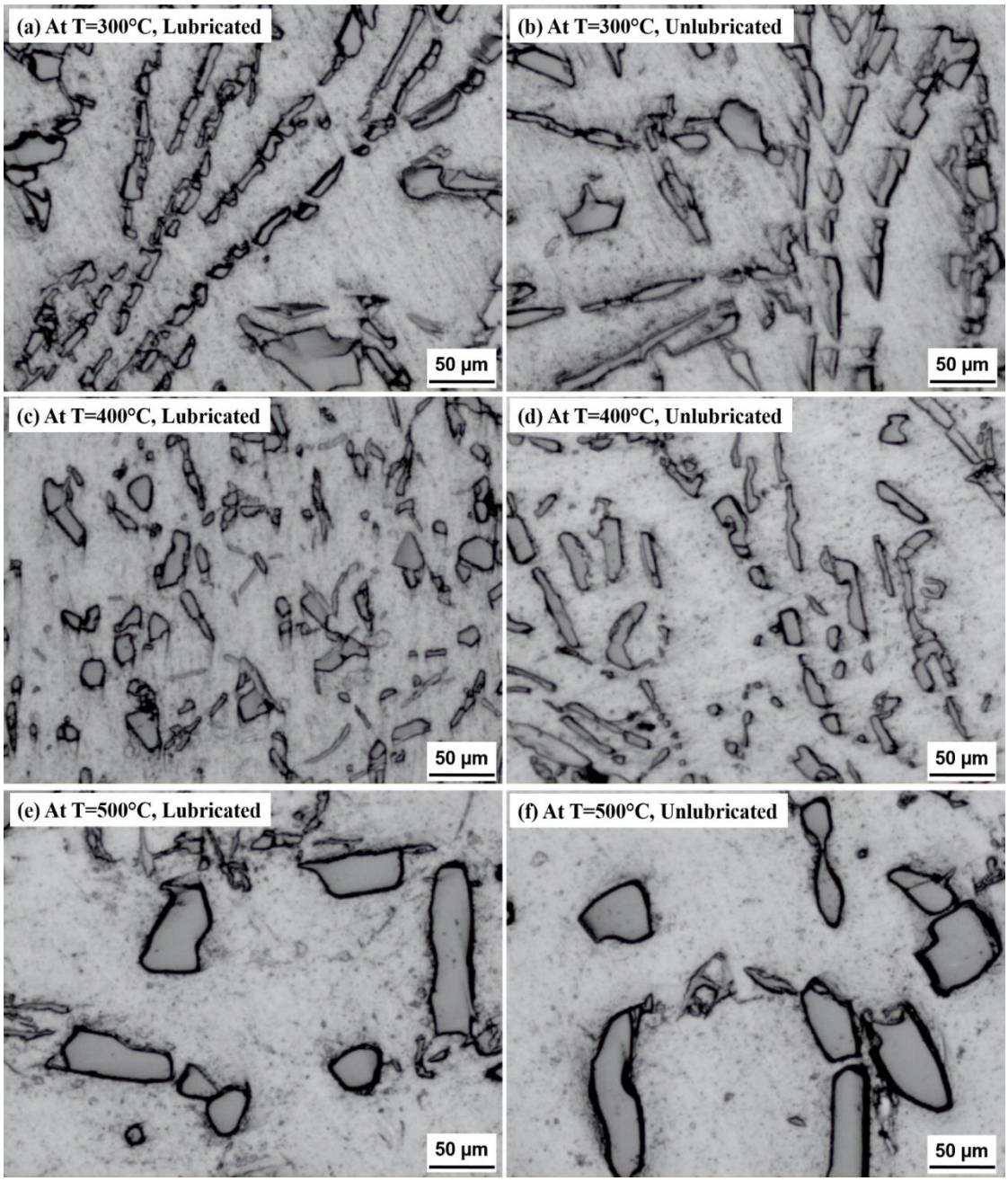

Figure 4.15 Optical microstructure of the forged samples at aspect ratio 1.0 under lubricated and unlubricated conditions

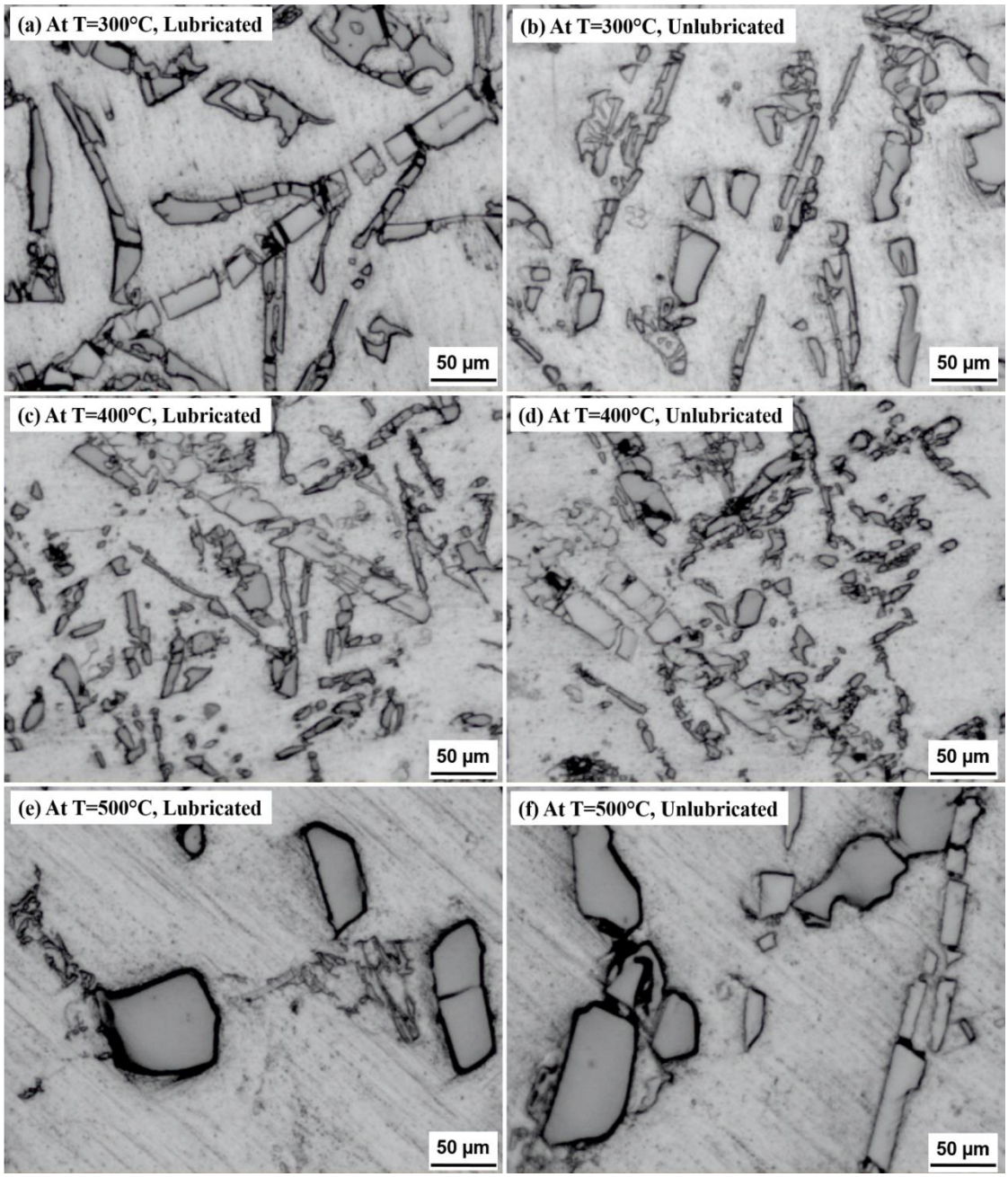

Figure 4.16 Optical microstructure of the forged samples at aspect ratio 0.80 under lubricated and unlubricated conditions

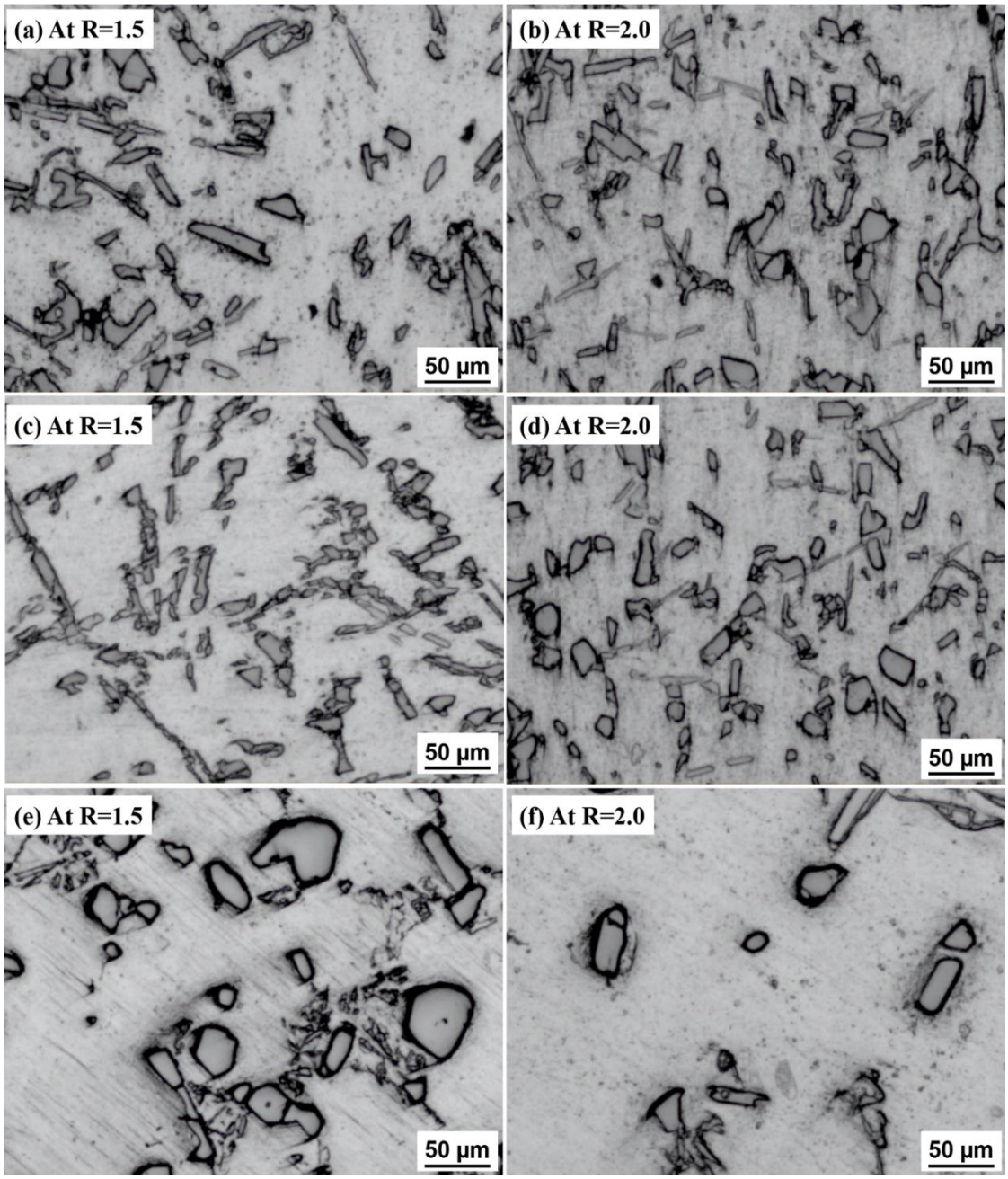

Figure 4.17 Optical micrographs of the forged billets (a) R=1.5, T=300°C, (b) R=2.0, T=300°C, (c) R=1.5, T=400°C, (d) R=2.0, T=400°C, (e) R=1.5, T=500°C, and (f) R=2.0, T=500°C

Tables 4.1, 4.2 and 4.3 show that average grain size of the Si particles in forged samples which significantly got reduced as compared to the as-cast alloy. The results reveal that degree of refinement increased with increase in the working temperature from 300 to 400°C (Figures 4.14-4.16(a-d)). While further increase in the working temperature from 400 to 500°C causes coarsening of the silicon particles (Figures 4.14-4.16(e-f)). It may

be due to a decrease in the yield strength of the alloy. Further increase in the working temperature results in higher deformation of the alloy, while coarsening occurred at 500°C due to the faster rate of diffusion. The results also reveal that the degree of refinement increased with increase in the aspect ratio/reduction ratio. It attributes to the extent of deformation which got increased with an increase in the aspect ratio and it was higher at h/d=1.20 (35%) in impression die, whereas R=2.0 (51%) in converging die.

In impression die forging microstructural results indicate that lubricated conditions show much better grain refinement, but very slight variation in their size. The microstructural features indicate that 400°C was the optimum working temperature to obtain the refined second phase particles with uniform distribution in both impression die as well as converging die forging. While 300°C is found to be relatively low whereas 500°C is relatively high working temperature during forging.

Liu et al., 2011 reported that coarse microstructural features of the cast Al–12.7Si–0.7Mg alloy changed from refined structure through the extrusion process. It may be due to the uniform dispersion of the fragmented second phase particles in the matrix during the extrusion process. However, refined second phase particles coarsened due to higher processing temperature as reported by Hogg and Atkinson, 2005. It may due to the diffusion of the Si atom at higher processing temperature.

4.2.4 Mechanical properties of the forged complex eutectic Al-11Si-2.5Cu-0.6Fe alloy

4.2.4.1 Tensile strength of the forged alloy

Tensile tests of as-cast and forged samples were conducted and the ultimate tensile strength (UTS) of the as-cast alloy was found to be 111±4.5 MPa. Figure 4.18 depicts the engineering stress-strain curves of the as-cast and forged samples (lubricated conditions) with aspect ratios (R) 1.20 at 300, 400 and 500°C working temperatures. Figure 4.19 shows the UTS of the forged samples with aspect ratios of 1.00, 1.20, and 0.80 under

different processing temperatures. Also the engineering stress-strain curves of the as-cast and forged samples with reduction ratios (R) 1.5 and 2.0 at 300, 400 and 500°C working temperatures as shown in Figures 4.20 and 4.21.

The results reveal that the tensile strength of the alloy considerably enhanced during impression and converging die forging both. The forged material in both the die setups show almost similar stress-strain behavior during tensile testing of the alloy. The literature reveals that mechanical properties of the alloy depend on the microstructural characteristics. The material having coarse microstructural features shows poor mechanical properties and thus fails during initial straining (Li et al., 2016). Therefore, to achieve the desired mechanical properties such microstructural features need to be eliminated. The microstructural features of the complex alloy got refined during bulk processing of under different processing conditions.

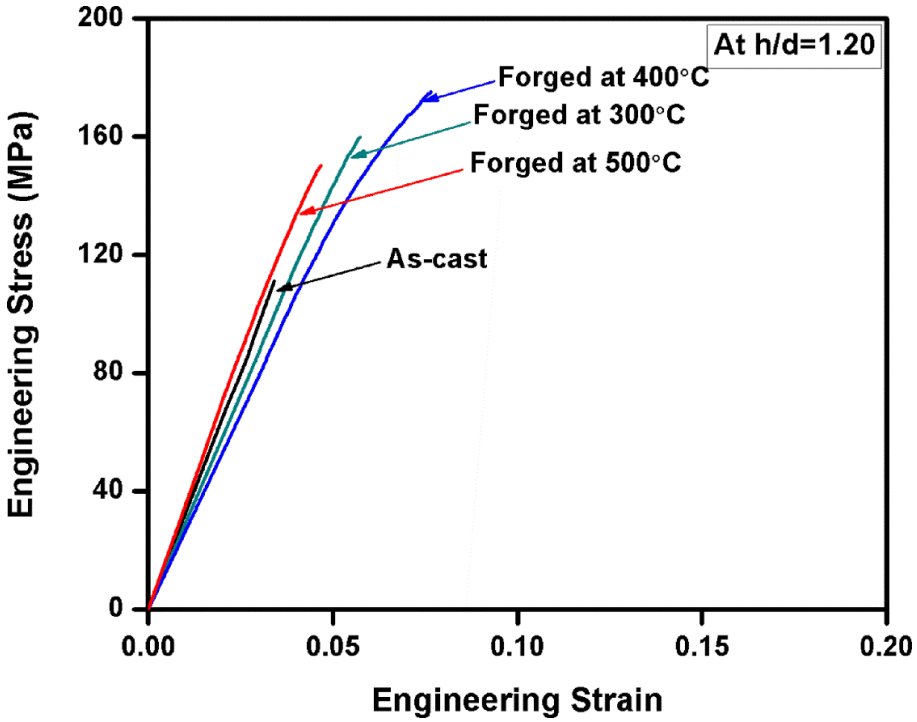

Figure 4.18 Stress-strain diagrams of the as-cast and forged samples (h/d=1.20)

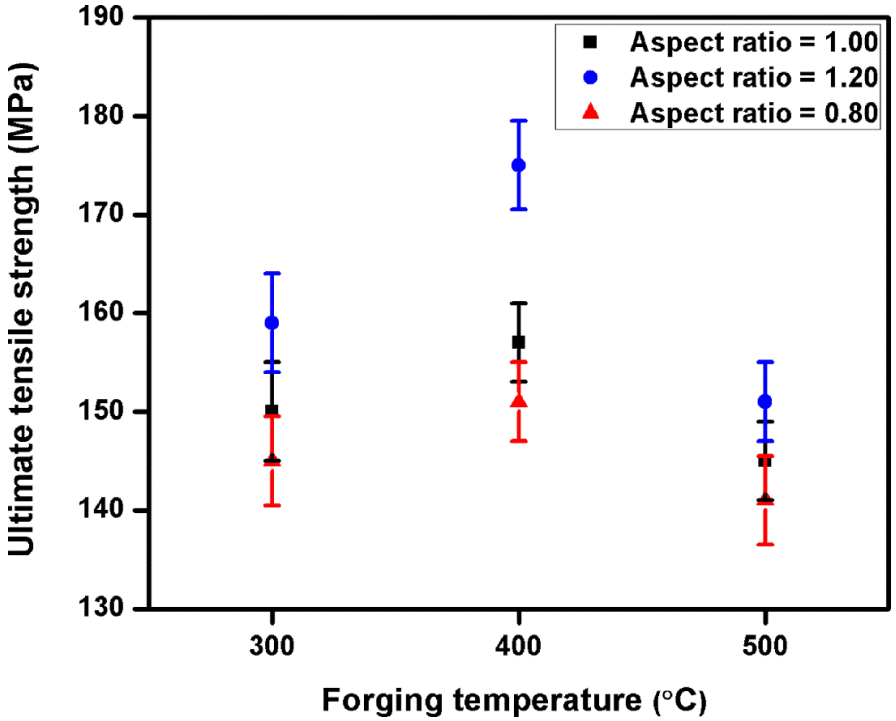

Figure 4.19 Ultimate tensile strength (UTS) of the forged samples shown against different h/d ratios and working temperatures (°C) under lubricated condition

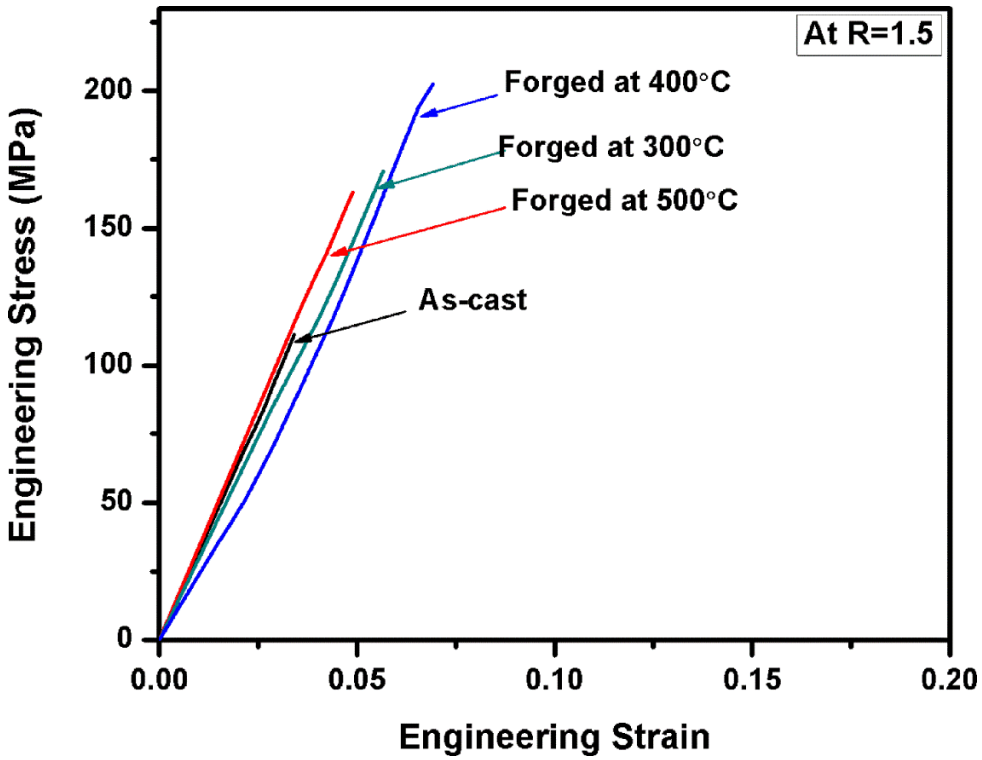

Figure 4.20 Stress-strain diagrams of the as-cast and forged samples (R=1.5)

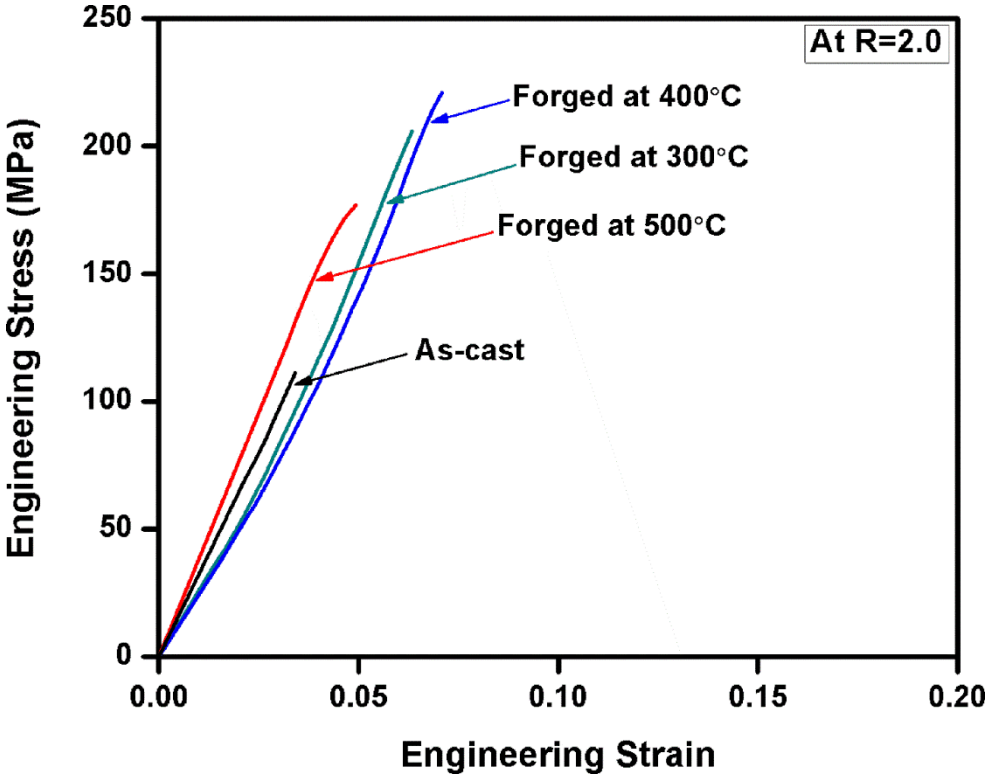

Figure 4.21 Stress-strain diagrams of the as-cast and forged samples (R=2.0)

Figures 4.18, 4.20 and 4.21 show a brittle fracture in all the cases and there was almost no plastic deformation. The deformation was essentially elastic in nature and therefore only the ultimate tensile strength is shown in these Figures 4.18, 4.20, and 4.21. As explained earlier that presence of the hard and complex intermetallic phases in the matrix lowers the tensile properties of the alloy and in turn failed without any plastic deformation. The XRD results also confirmed the presence of the similar intermetallic compound of the iron (β-$Al_{4.5}$FeSi) in the complex Al-11Si-2.5Cu-0.6Fe (wt.%) alloy. Due to these intermetallic phases, the failure of the alloy was similar to that of hypereutectic Al-18Si-2.5Cu-0.6Fe (wt.%) alloy.

However, the Figures 4.18-4.21 show significant improvement in tensile strength alloy forged under different processing conditions. It may be due to the microstructural refinement in the alloy during forging process. Such refined second phase particles develop strong bonding with Al matrix and make a strong the alloy as per the Hall-Petch strengthening mechanism. As explained in the previous section (3.2.4) that tensile

strength decreased due to the faster rate of diffusion and also grain growth of the matrix at a higher processing temperature (500°C) during forging. Here also observed the decrement in the strength of the alloy forged at 500°C. Previously, Jung et al., 2016; and Suryawanshi et al., 2016 reported that coarse second phase particles in the matrix lower the tensile properties of the other eutectic Al-Si alloy by initiating micro-cracks during straining which in turn failure of the test samples. However, alteration of such coarse microstructure to refined grains considerably enhanced the tensile properties of the alloy. Figures 4.19-4.21 also confirmed that UTS of the forged alloy depends on the aspect ratio or reduction ratio during forging. It is attributed to the higher percentage of deformation of the alloy during forging with an increase in either aspect ratio (h/d) or reduction ratio (R). Therefore, the alloy deformed with higher aspect ratio 1.20 (35% deformation) in impression die and higher reduction ratio 2.0 (51% deformation) in converging die show higher UTS as compared with other conditions. Such deformation generates a high density of dislocation and also refines the microstructure which leads to considerable improvement in UTS of the forged alloy. Further, the alloy forged through converging die indicates greater improvement in UTS as compared with impression die. It may due to greater microstructural refinement during processing in all working temperatures.

4.2.4.2 Hardness

Hardness tests of the as-cast and forged samples were conducted through Vicker's microhardness tester at 100 g indentation load and 10 sec dwell time. The hardness of the as-cast was found to be 51±3HV. The results reveal that the hardness value of the alloy significantly enhanced during forging in both impression die as well converging die in all processing conditions as shown in Figures 4.22 and 4.23, respectively. Due to the similar processing conditions used in both the forging processes, the improvement phenomenon in the hardness value of the forged alloy was quite similar. Figures 4.22 and 4.23 also show that the increment in processing temperatures from 300 to 400°C during

forging increase the hardness value of the forged alloy, while at the higher temperature (500°C) it decreased due to coarsening of the microstructural features.

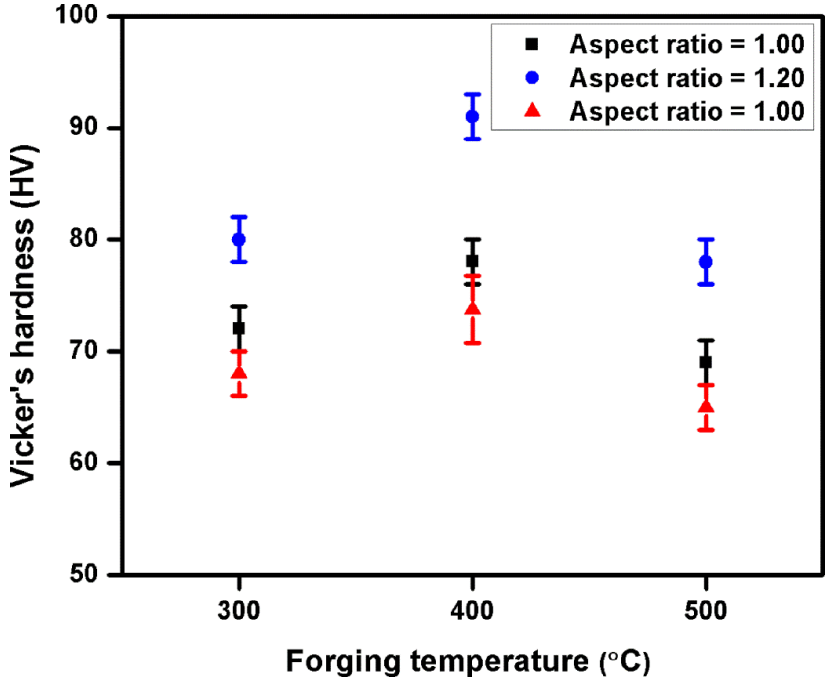

Figure 4.22 Vicker's microhardness of the forged samples shown against different h/d ratios and working temperatures (°C) under lubricated condition

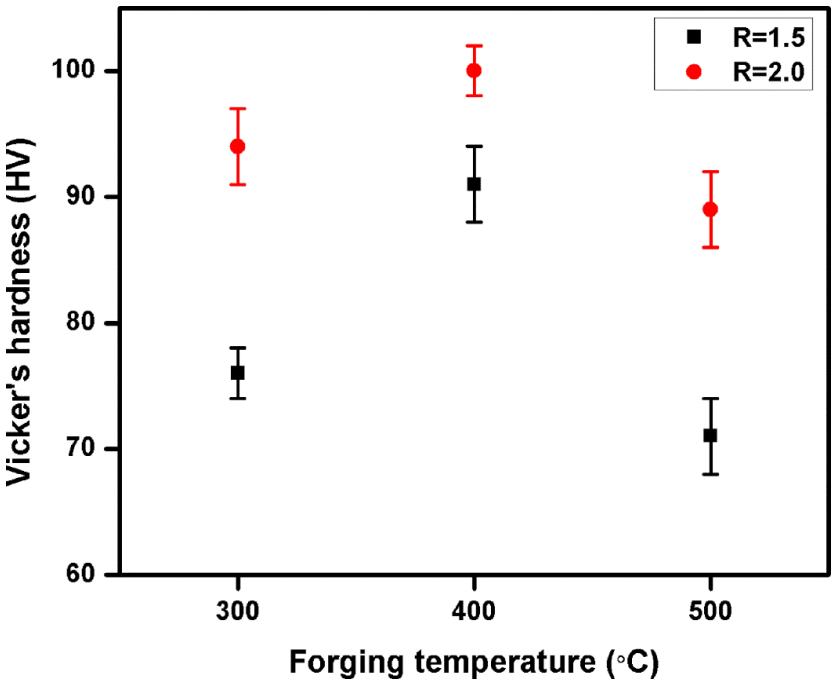

Figure 4.23 Vicker's microhardness of the samples forged to different reduction ratios (R) of 1.5 and 2.0 at different working temperatures

The hardness improvement phenomenon of the forged alloy was quite similar as discussed in the previous sections 3.2.4.2. It may be due to increase in dislocation density

during forging at high strain rate and more uniform dispersion of the second phase particles in Al matrix. In the earlier section, it was reported that microstructural refinement and higher dislocation density enhanced the hardness of the alloy.

4.2.4.3 Fractography

The tensile fractograph of the as-cast alloy is shown in Figure 4.24. The fracture morphology of as-cast alloy reveals that material failed due to brittle failure with insignificant plastic deformations during straining. The fracture surface shows a large area of cleavage facet along with fractured primary Si in the failed samples. The brittle fracture occurred in the material due to the presence of the coarse and needle shaped second phase particles in the alloy matrix. In these conditions, the alloy having coarse and needles shaped eutectic and intermetallic phases along with some primary Si particles, which generates high stress concentration with Al matrix during straining. Due to this micro-cracks formed in the matrix near the second phase particles which further propagated during loading. Thus, the material failed at higher load during testing.

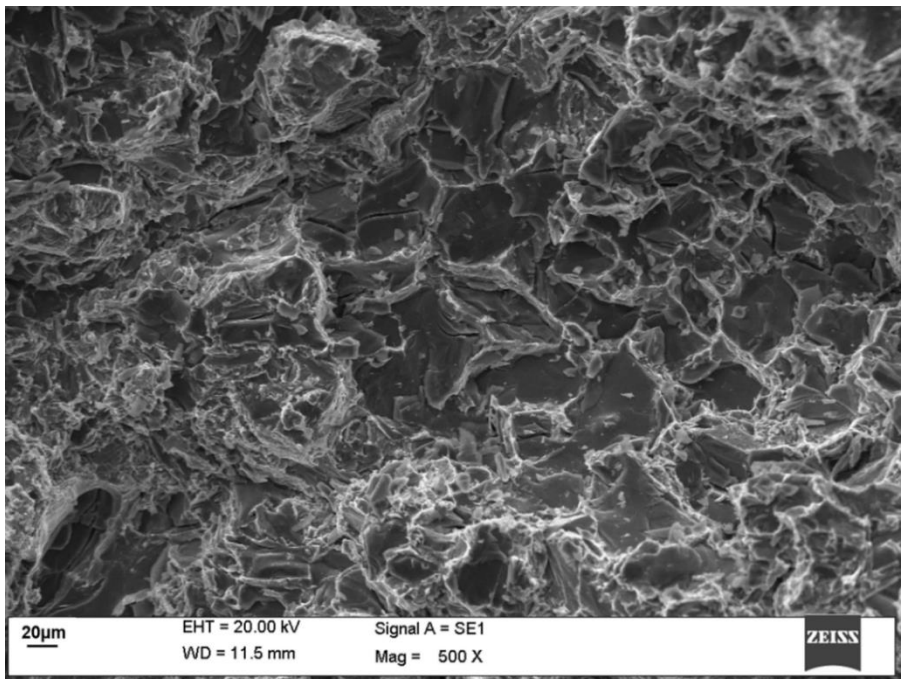

Figure 4.24 SEM image of the as-cast tensile fractured surface

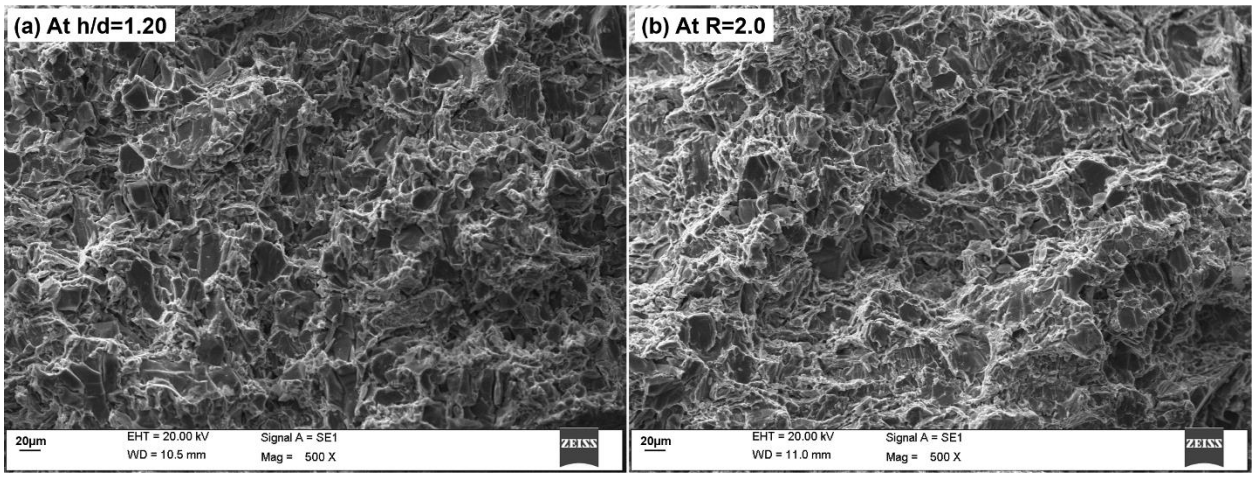

Figure 4.25 SEM images of the fractured surface at 400°C working temperature for aspect ratios (a) 1.20 and (b) 0.80

Figures 4.25 (a-b) depict the fractured surface morphology of the failed samples forged at 400°C with the aspect ratio (h/d) of 1.20 and a reduction ratio of 2.0. The fracture morphology of both the forged failed samples also shows brittle fracture having facet and cracked Si particles. The bulk forming refines the coarse morphology of the second phase particles as seen the microstructural results, even then the forged material suffers a brittle fracture. It may be due to the presence of hard intermetallic of Fe rich compound and Si particles reduce the ductility of the alloy. Therefore, up to some extent the load carrying capacity of alloy increases but at the same time, the micro-cracks were also formed in the matrix near to the second phase particles. Thus, the sample failed at higher load due to the further propagation and separation of the cracks in the matrix having very few shallow dimples.

Various investigators also reported a similar fractography trend in Al-Si alloy with other chemical composition processed through some different techniques. It was found that brittle fracture occurred in the alloy due to the presence of the coarse second phase particles and their random distribution in the matrix. Such particles generates high stress concentration with the Al matrix during loading and produces cracks. Tutunchilar et al., 2012; Li et al., 2016; and Han et al., 2017 found that base Al-Si alloy with eutectic

compositions show brittle fracture during straining. The fracture morphology contains large facet area and cleavage planes disconnected by tearing ridges. Wang et al., 2014 found the few shallow dimples in the fracture surface of the extruded eutectic Al-Si alloy during tensile testing.

4.2.5 Wear behavior of the as-cast and forged complex eutectic Al-11Si-2.5Cu-0.6Fe alloy

The results reveal that mechanical properties of the forged alloy depends on the microstructural features, and it is higher for the samples having refined second phase particles. Therefore, wear tests were performed under dry sliding condition to study the effect of the bulk processing parameters on wear characteristics of Al-11Si-2.5Cu-0.6Fe alloy.

The results show that tensile strength and hardness of the forged alloy significantly enhanced in the both die conditions, and depicts almost similar behavior. Due to this, it is expected that wear behavior of the forged alloy will also be same. The alloy forged through converging die shows better refined second phase morphology as compared to impression die. Therefore, samples were prepared from the converging die forged billets and wear tests were conducted as per the experimental techniques discussed in section 2.8

4.2.5.1 Wear behavior of the as-cast and forged alloy through converging die

Figures 4.26 and 4.27 depict the variation in cumulative weight loss against sliding distance of the as-cast and forged samples with R=1.5 and 2.0 at applied normal load 20 N. The results show that cumulative weight loss of the test samples increased with increase in sliding distance. The results reveal that weight loss was initially low but it suddenly increased with increase in sliding distance as shown in Figures 4.26 and 4.27. Results also show that weight loss was low for the forged samples as compared to as-cast

alloy and it was minimum for sample with 2.0 reduction ratio and 400°C forging temperature.

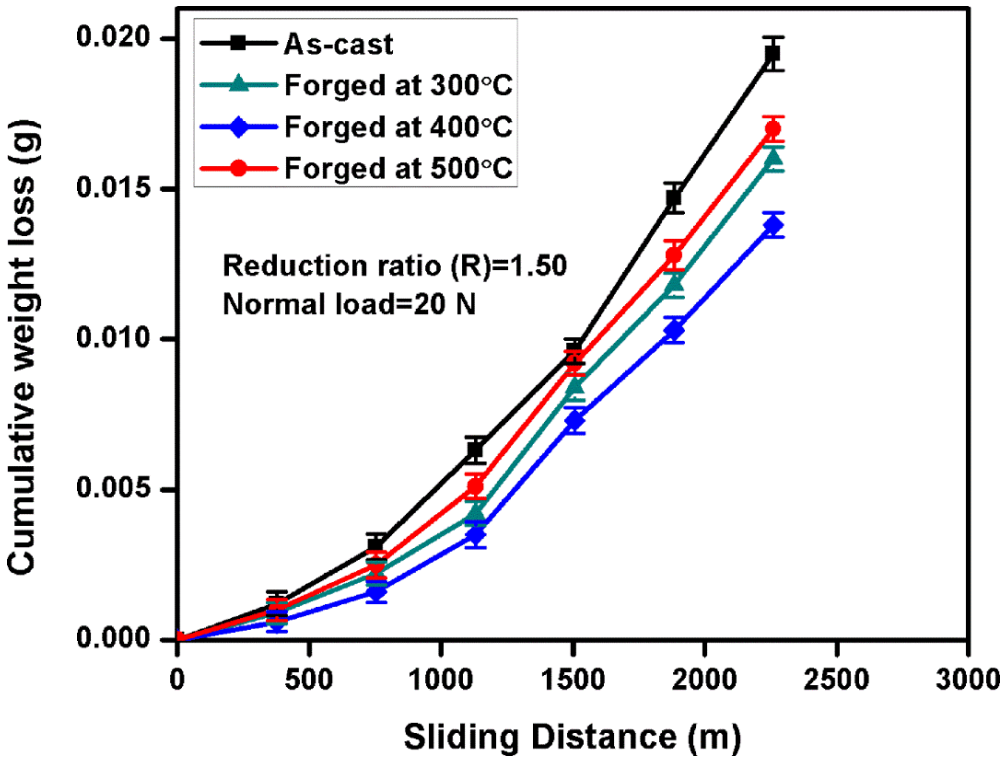

Figure 4.26 Cumulative weight loss of the as-cast and forged samples (R=1.5) under different conditions

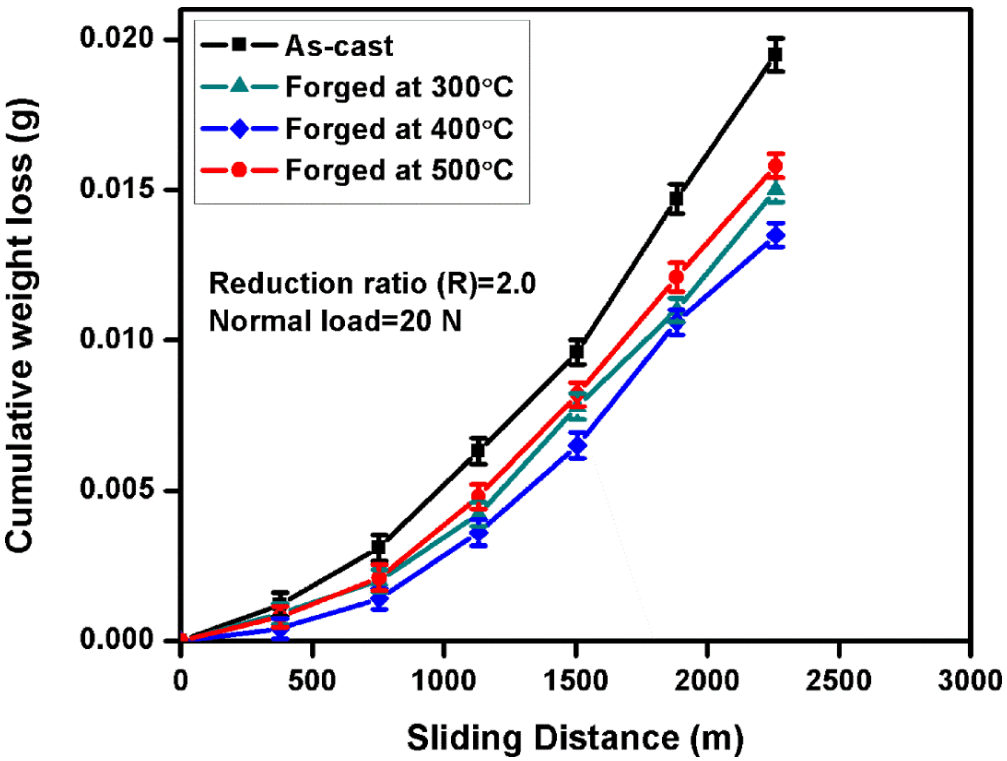

Figure 4.27 Cumulative weight loss of the as-cast and forged samples (R=2.0) under different conditions

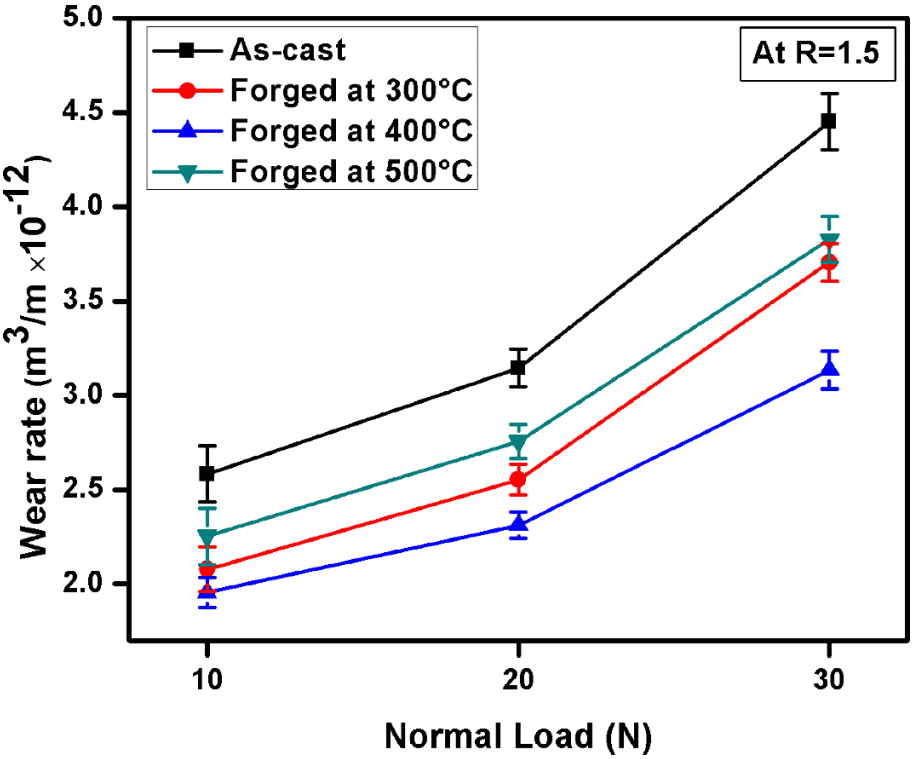

Figure 4.28 Wear rate of the as-cast and forged samples at R=1.5 and 10, 20, 30 N normal loads

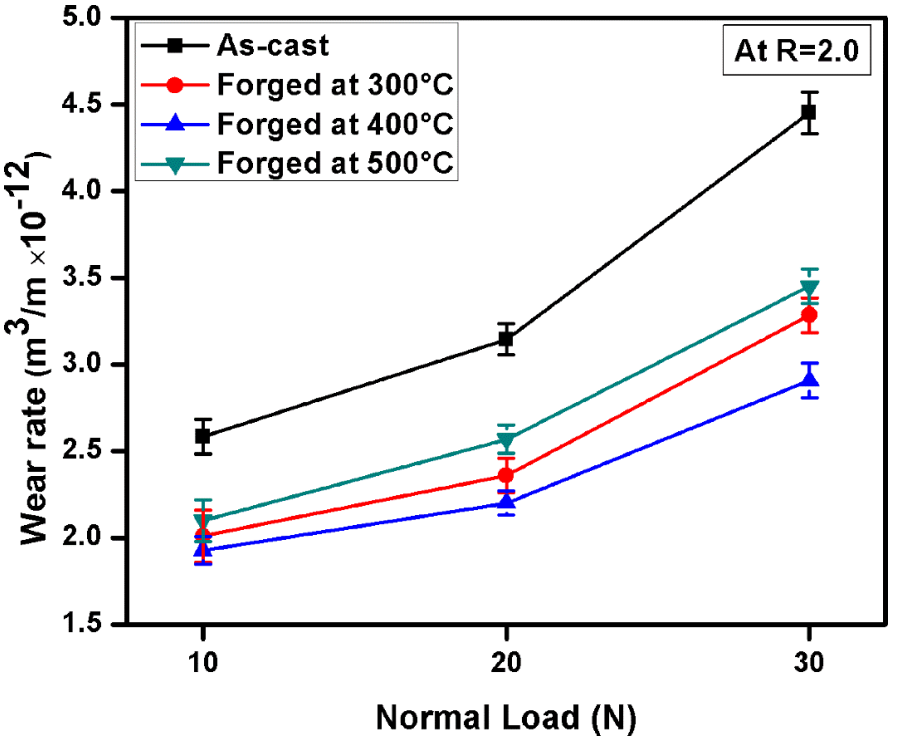

Figure 4.29 Wear rate of the as-cast and forged samples at R=2.0 and 10, 20, 30 N normal loads

Figures 4.28 and 4.29 show the variation of wear rate with the applied normal load for the as-cast and forged samples respectively. The wear test of the as-cast, and forged test

samples with 1.5 and 2.0 reduction ratios at 300, 400 and 500°C temperatures were conducted for constant sliding velocity and distance of 1.3 m/s, and 2260 m respectively. The results reveal that wear resistance of the forged complex alloy noticeably improved as compared to as-cast alloy. It may be due to higher hardness of the forged samples as compared to as-cast alloy. This reduces the plastic deformation of the test samples which in turn decreases the mass loss of the alloy. Figures 4.28 and 4.29 reveal that wear rate of as-cast alloy abruptly increases at an applied normal load of 30 N, while it is considerably low for forged alloy under same test conditions. It was attributed to the severe plastic deformation of the material at higher applied load. The results also reveal that wear resistance of the alloy increased with increase in reduction ratio (R) and forging temperatures from 300 to 400°C. However, further increase in forging temperature from 400 to 500°C reduces the wear rate of the alloy. It may be due to lower hardness value of the forged samples at 500°C which deformed slightly more during sliding and results in increase of mass loss of the material.

Various authors also reported the similar wear trend in the eutectic Al-Si alloys having different other chemical compositions. It may be found in the studies that wear rate in the as-cast alloy was higher due to coarse microstructural features, and it significantly increased with increase in the applied pressure. It may be also revealed that some modification in the microstructure of the alloy considerably improved the wear resistance of the alloy (Wang et al.; 2004; and Kucukomeroglu, 2010).

4.2.5.2 Wear Mechanism

Scanning electron microscopy of selected worn samples was done to analyze the material loss mechanism during dry sliding conditions. Figures 4.30 and 4.31 depict the worn surface morphology of the as-cast and forged samples under different testing conditions of applied load, and sliding distance.

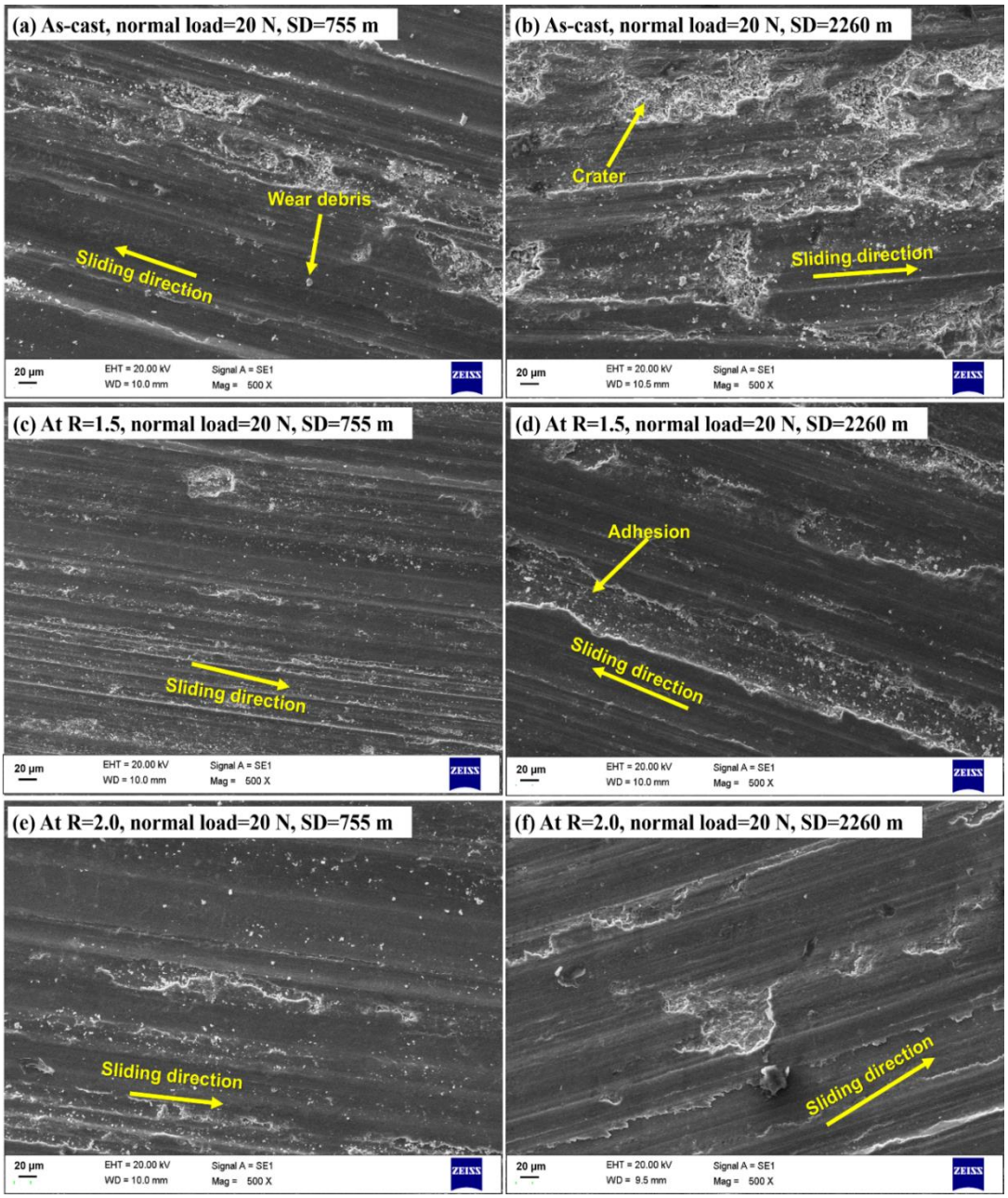

Figure 4.30 Worn surface morphology of the as-cast and sample forged at 400°C, at constant applied normal load of 20 N, sliding velocity of 1.3 m /s for different sliding distances

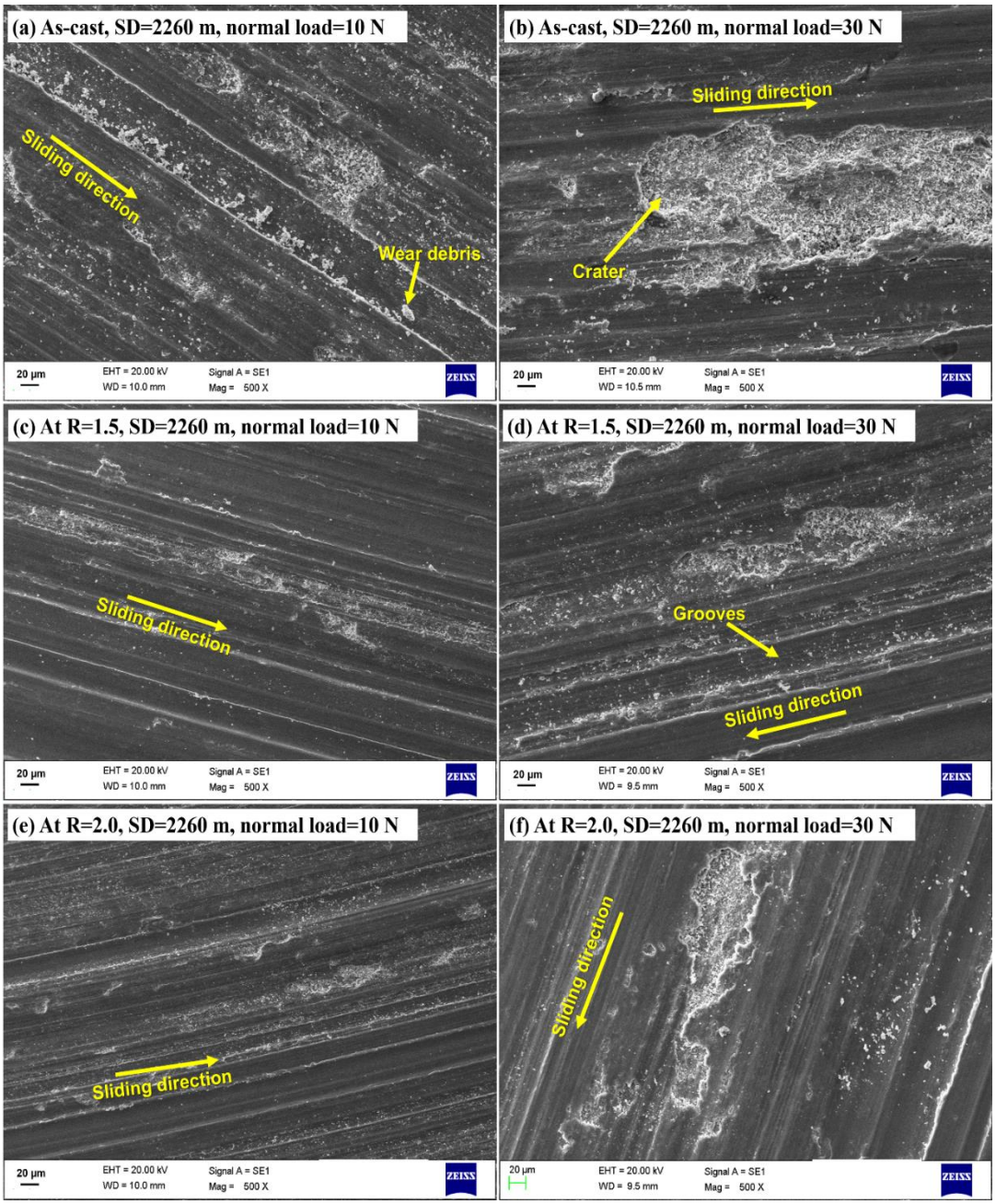

Figure 4.31 Worn surface morphology of the as-cast and samples forged at 400°C, at constant sliding distance of 2260 m, sliding velocity of 1.3 m /s for different applied normal loads

Figure 4.32 shows the EDS spectrum of the worn surface of the forged alloy (R=2.0 at 400°C) at 30 N normal load and sliding distance of 2260 m. The EDS spectrum reveals that worn surface contains the alloying elements of the material such as Si and Cu, while Fe transfer from the counter surface during dry sliding. The EDS spectrum of the worn surface also indicate that no additional compound were formed during rubbing of the interacting surfaces.

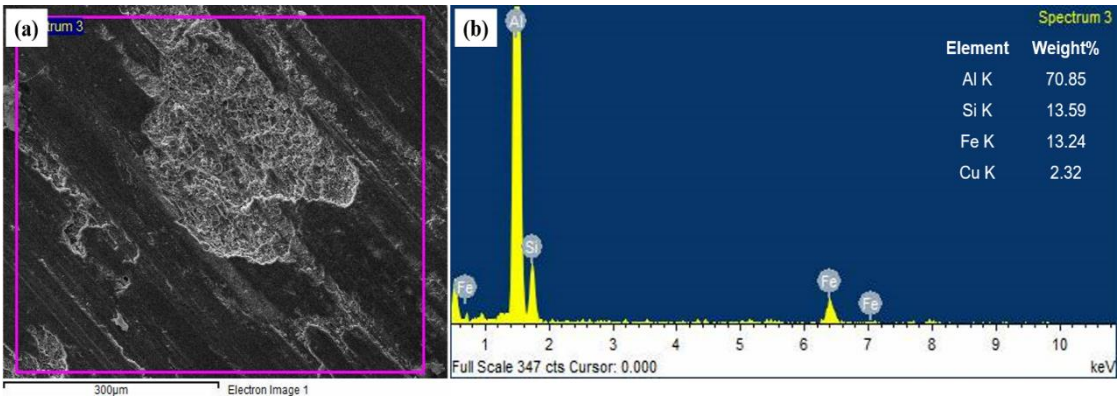

Figure 4.32 EDS analysis of the worn surface of the sample forged at R=2.0 and 400°C at 30 N normal load and sliding distance 2260 m

Figures 4.30(a-f) show the worn surface morphology of the as-cast and forged samples (R=1.5 and 2.0 at 400°C) at constant normal load (20 N) and sliding speed of 1.3 m/s for different sliding distances (SD=755 and 2260 m). The results show that the severity of wear increased with the sliding distance which indicates that wear changes from mild to severe during dry sliding conditions. Figures 4.30(a-f) reveal that abrasion and adhesion were the main wear mechanism in the as-cast and forged alloy during the dry sliding condition. Grooves, ridges and crater were also observed on the worn surfaces parallel to the sliding direction. Figures 4.30(a-f) show that the severity of wear was higher at 2260 m sliding distance in all wear samples. It may be attributed to high localized heat produced due to friction between interacting surfaces during sliding which soften the pin material. Due to softening, the material deformed plastically during sliding and detached from the pin surface which produced deep craters in the pin surfaces. Some of the detached particles come in the contact zone of sliding surfaces and act as a third body abrasive particles which increase the material loss though micro-cutting. The deeper and wider grooves were formed on the pin surfaces due to the penetration of hard asperities of the counter disc during sliding. It may be attributed to the softening of the material due to localized frictional heat generation which led to deeper penetration of asperities and wider groves were formed on the pin surfaces. The worn surface of as-cast alloy shows

wider and deeper grooves, and crater as compared to forged alloy samples as shown in Figures 4.30 (a-f). It may be attributed to the higher hardness and refined second phase particles in the matrix of the forged samples which reduces the wear in the alloy.

The existing studies also reveal that material having coarse second phase particles easily worn out during dry sliding condition. It may be due to coarse particle morphology which leads to poor bond strength with the matrix and yields lower hardness of the material, while needle shaped second phase particles produce stress concentration with Al matrix and initiate micro-cracks during sliding. Such cracks were connected to each other and detach from the surface as wear debris (Chandrashekharaiah and Kori, 2009). Fine and uniformly dispersed second phase particles prevent the direct contact of the matrix and bear the applied load. The material having such microstructural features reduces the wear rate (Abouei et al., 2010a; and Chen et al., 2013). Therefore, the forged samples with higher reduction ratio show better abrasion and adhesion resistance during dry the sliding condition.

Figures 4.31(a-f) show the worn surface morphology of the as-cast alloy and the forged samples (R=1.5, 2.0 and 400°C) for a constant sliding velocity and distance of 1.3 m/s and 2260 m respectively, for varying applied normal loads of 10 and 30 N. The results reveal that the severity of the wear increased with increase in applied normal load. In the previous section 3.2.4, it was explained that penetration of hard asperities into the soft Al matrix increases with increase in applied normal load, which in turns lead to more plastic deformation of the soft material. Therefore, more wear rate was observed at higher applied normal load due to the bulk amount of the material loss during dry sliding. Along with this, some of the hard fragmented or squeeze out second phase particles act as third body abrasives and enhances the material loss through micro-cutting.

Figures 4.31 (a-f) depict that deeper and wider grooves were formed on the pin surface when the applied load was increased. It may be due to greater braking energy at higher

applied normal load as discussed in the previous section 3.2.4, which increases friction between contacting surfaces and generate a large amount of heat. Therefore, such frictional heat leads to softening of the material due to which it deformed plastically when load was applied. Thus, the deeper grooves were formed on the surface of the as-cast alloy, while shallow grooves were formed on the forged sample surface. It may be due to higher hardness value of the forged samples. This reduces the plastic deformation of alloy during sliding. Therefore, abrasion and adhesion were the primary wear mechanism in the as-cast and forged alloy. Earlier Anasyida et al., 2010; and Basavakumar et al., 2009 were also found the similar wear trend eutectic Al-Si alloys with other chemical compositions. It may be reported that deeper and wider grooves along with crater were formed in the pin surface at higher applied pressure.

4.2.5.3 Roughness measurement

Figure 4.33 shows the three dimensional AFM images and their respective roughness profiles of the worn surfaces of the as-cast and forged alloy with reduction ratios (R) 1.5 and 2.0 for the scanning area of 50 µm × 50 µm for each sample.

The root mean square (rms) roughness (Rq) of the as-cast worn surface was measured from AFM analysis and it was found to be 0.670 µm as shown in Figure 4.33(a) while, it were 0.430 and 0.375 µm for the worn surface of the forged sample with reduction ratios of 1.5 and 2 respectively as shown in Figures 4.33(b) and 4.33(c). These results reveal that roughness value of the test samples depends on the hardness of the test samples, and a material exhibit poor surface roughness characteristics having low hardness value. Therefore, the forged worn samples show low surface roughness as compared to as-cast alloy as shown in Figures 4.33(a-c). It may be attributed to the improvement in hardness of the alloy during forging, which reflects the low wear of the forged materials during dry sliding as depicted by Archard's law (Abouei et al., 2010b). Results also reveal that

surface roughness (Rq) of the worn forged samples also decreased with increase in reduction ratio as shown in Figures 4.33(a-c).

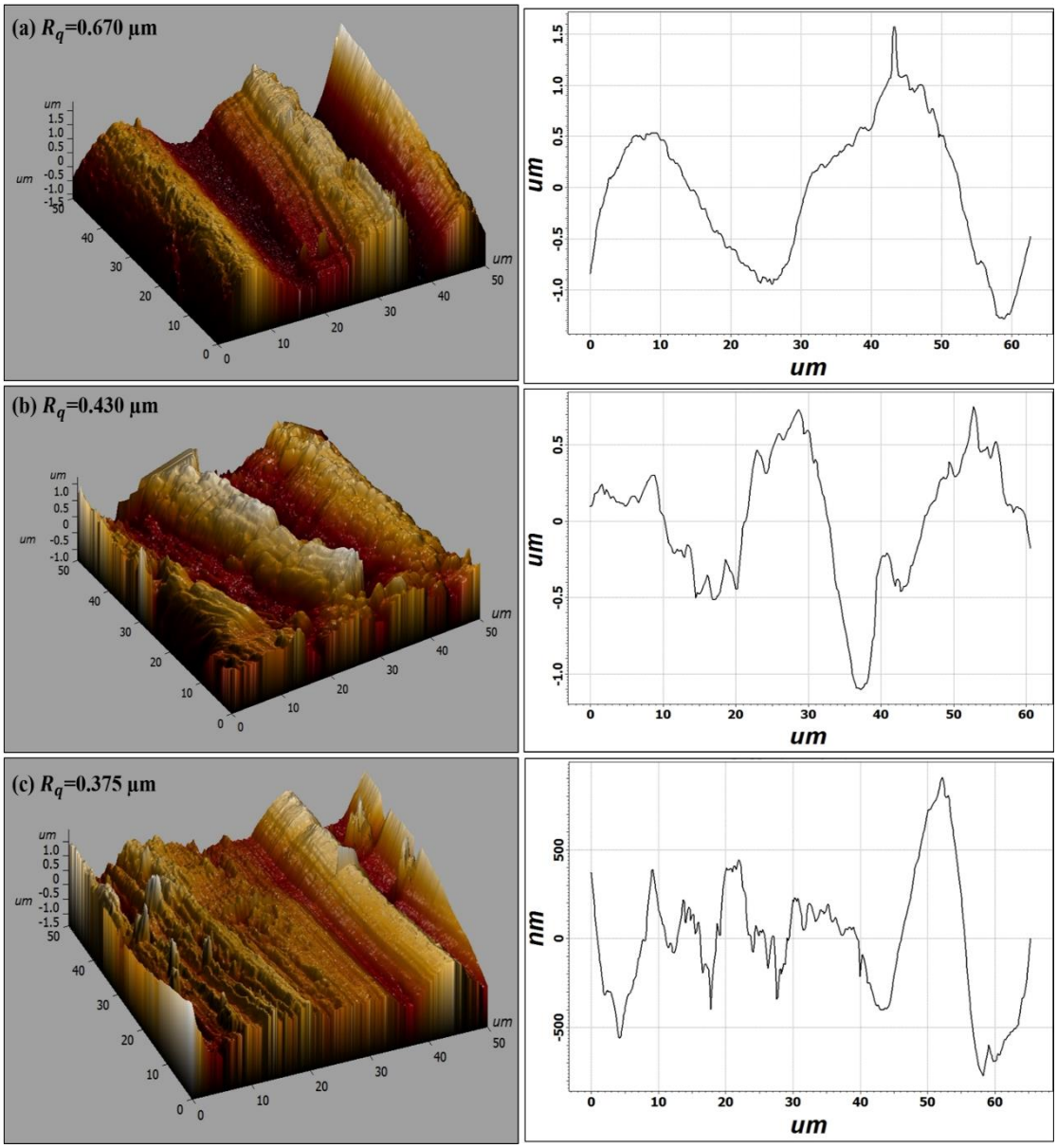

Figure 4.33 AFM morphology of worn surfaces at sliding distance of 2260 m, sliding velocity of 1.3, and applied normal load of 20 N for the different samples (a) as-cast, (b) forged R=1.5 at 400°C, and (c) forged R=2.0 at 400°C

The roughness profile shows that peak height and depth of penetration was very high for as-cast worn sample, and it was found to be ≈1285 and ≈1570 nm as shown in Figure 4.33(a) while it reduced significantly in the forged sample, and found to be ≈1103 & ≈750 nm for sample with R=1.5 and ≈771 & ≈906 nm for R=2.0 as shown in Figures 4.33(b)

and 4.33(c), respectively. It may be due to the lower surface roughness of the forged worn samples which reflect the low peak height and depth of the penetration.

4.3 Summary

The important findings of the above work are summarized below:

1. The open die forging of the alloy at room and elevated processing temperatures, and the impression die forging of the alloy at room temperature in both lubricated and unlubricated conditions was not feasible and the cracks were visible on the outer surface of the products.
2. The defect free smooth forged products were obtained in the impression die forging of the alloy at elevated temperatures (300°C, 400°C and 500°C) with different aspect ratios (h/d=1.20, 1.00 and 0.80) in both lubricated and unlubricated conditions.
3. The defect free forged products were also obtained in converging die forging of the alloy at reduction ratios of 1.5 and 2.0, and elevated processing temperatures.
4. In impression die forging of the alloy in both lubricating conditions, it was observed that forging load increases with an increase in the aspect ratio of the samples.
5. Bulk processing lead to microstructural refinement in the forged samples. It may be due to fragmentation and uniform dispersion of the second phase particles in the laterally flowing Al matrix with the effect of the applied load.
6. At 400°C, the samples forged with 1.20 aspect ratio in impression die and 2.0 reduction ratio in converging die depicts optimum refinement in microstructural features as compared to other processing conditions. Coarsening occurred in the microstructural features at 500°C processing temperature during forging.

7. The refinement in microstructural features led to significant improvement in tensile strength and hardness of the forged alloy. The UTS and hardness of the alloy were optimum when it forged with aspect ratio of 1.20 in impression die, and reduction ratio of 2.0 in converging die at 400°C.
8. Wear resistance of the alloy considerably improved during the forging process. The surface morphology of the worn samples reveal that adhesion and abrasion were the dominant wear mechanisms in the as-cast and forged samples. The AFM analysis depicts that surface roughness was minimum for the forged samples as compared to as cast alloy.

The next chapter 5 deals with deformation behavior and tribo-mechanical properties of the complex hypereutectic Al-7.4Si-2.5Cu-0.6Fe alloy during forging.